

### **(Editor)**

The article has been reviewed by two referees who both support the modelling effort in this study. Both underline that the study should be published after minor or moderate modifications. The clarity of the definition of fracture (breakdown) energy could be readily improved, in addition to the comparison with the quasi-steady-state solution given by previous studies. All the TP modelling work (as in the present study) use constant TP coefficient, which makes the pressurization so efficient that tends to cause a nearly-complete stress drop (at least in the spring-slider model). I am wondering what could be the possible damping factor(s) for the TP process (e.g., a smaller TP effect with decreasing effective normal stress). Would these factors affect the fracture energy and the rupture process? This would need extra work, but it will be useful if the authors could at least comment on this.

The emphasis of this work is to demonstrate that even in fault models with constant and uniform TP parameters, the resulting breakdown energy is heterogeneous and not constant in time, thus it is rupture-dependent. Given suggestions from the reviewers, we now expand on this to discuss the importance of dynamic rupture simulations for evaluating the variability and physical interpretation of breakdown energy in fault models with thermo-hydro-mechanical processes, compared to steady-state rupture solutions.

The TP parameters used in this work represent moderate weakening motivated by our previous work and other prior studies (e.g. Rice, 2006), and do not result in complete stress drop (as is seen Figures 5-10). These parameters have also been shown in our prior studies to be able to qualitatively and quantitatively reproduce a number of seismological observations, including magnitude invariant static stress drops between 1-10 MPa, the inferred scaling and values of breakdown energy from moderate to large earthquakes, and radiation efficiencies between 0.1 to 1 (Perry et al., 2020; Lambert et al., in review). These studies suggest that fault models with such TP parameters may be plausible representations of natural mature faults, at least megathrust faults.

Indeed, heterogeneous and non-constant hydraulic properties, as may result from damage generation during rupture, would further complicate the evolution of shear stress with thermo-hydro-mechanical processes like TP, as was already discussed in lines 312 – 317 of the original manuscript (now 115- 119 and 434 - 439). As damage generation is also likely to be rupture-dependent, this is also expected to reinforce our conclusions that breakdown energy is rupture-dependent, as discussed in the conclusion section.

### **Referee 1 (E. M. Dunham)**

This study examines the dependence of dissipated energy on rupture history using simulations of earthquake ruptures with thermal pressurization as the dominant fault weakening mechanism. Dissipated energy can be divided into work done by sliding against the residual strength of the fault (referred to in this study as dynamic strength) and breakdown energy. Breakdown energy is one of the few earthquake source properties that can be indirectly estimated from far-field seismic radiation, and numerous observational studies have explored the dependence of breakdown energy on earthquake magnitude, local slip, etc. Likewise, theoretical studies of proposed fault weakening processes, like thermal pressurization, provide predictions of how breakdown energy depends on slip and various parameters (like thermal and fluid transport properties of the fault zone). However, in order to obtain closed form analytical solutions, these theoretical studies often make assumptions like constant slip velocity, that are unlikely to be met in reality. The current study utilizes more complex earthquake simulations with thermal pressurization that provide more realistic rupture and slip histories. The authors calculate breakdown energy, both locally at each point on the fault and in a suitably averaged sense, and compare to both theoretical predictions and observational constraints.

The main conclusions are that local breakdown energy can exhibit large spatial variations across the fault, due the complex rupture history, and can be quite different from the average breakdown energy that is estimated from far-field seismic observations. The study thus provides an important caveat for

researchers who hope to infer fault weakening mechanisms from seismic observations. The study is well designed and the manuscript is clearly written; I recommend publication after addressing the following minor comments:

Thank you for the positive assessment of our work and comments that helped us improve the manuscript. Please find our responses to your comments below.

1. Line 45. It is stated that peak and dynamic strengths are expected to be material properties of a fault, but I disagree that this is how people usually think about it. It is more common to regard static and dynamic friction coefficients as material properties, recognizing that shear strength depends on both friction and effective normal stress. I think it is widely understood that the ambient effective normal stress is not a material property of fault, but depends on tectonic loading and fluid state. I recommend explaining this in more detail, pointing out that for the set-up in your 2D simulations, the ambient effective normal stress is a prescribed quantity that is unaltered by fault slip (unlike in a dipping fault configuration, etc.).

We agree that the statement is imprecise and it is not essential to the manuscript so we have removed it. We have added the discussion about potential variations in ambient effective normal stress.

2. Line 53. The LEFM relationship between rupture velocity and breakdown energy requires that the small-scale yielding criterion is met. You later explain this, but it might be helpful to mention small-scale yielding here. (Optional)

We have added this specific example where small-scale yielding is introduced on line 84 (now 98).

3. Line 60. I think you mean greater than 1 m/s, not  $10^3$  m/s!

We have corrected the text with the correct value  $10^{-3}$  m/s or 1 mm/s, which generally represents the initiation of enhanced weakening in the lab. Thank you for noting this typographical error.

4. Line 136. “or” should be “of”

Thank you.

5. Equation (11). Should the integral be over Sigma, not Omega? In any case, please make sure to define Sigma and/or Omega.

We have updated the notation to consistently use Omega to denote the ruptured domain and clarified this in the text.

6. Line 194, lines 258-260, line 339, and elsewhere. (Depending on how you choose to respond to this suggestion, this could warrant a major revision.) You compare your simulation results to the two closed-form thermal pressurization solutions in Rice (2006), both of which utilize the constant slip velocity assumption. However, this was improved upon by Viesca and Garagash (2015) to account for a more realistic slip velocity history that accounts, in the context of a steadily propagating rupture, for elastodynamic relations between slip and stress change. Viesca and Garagash also provide solutions for thermal pressurization and the dependence of breakdown energy on slip. I think your paper would be substantially strengthened by comparing your simulation results to their theoretical predictions, in addition to the Rice (2006) predictions. This might provide insight into the validity of a steady state solution for describing more complex ruptures that accelerate, decelerate, interact with arrest waves, etc. Perhaps there are situations where the steady state solution is a good approximation, or maybe not. It would be very useful to know this since it will help guide the field to either invest more time in developing steady state solutions for other weakening mechanisms or to instead shift toward fully numerical rupture simulations like you have done.

This is an excellent suggestion that we have implemented in the manuscript. The approximation of a steadily propagating rupture does not capture the variability in local  $G$  vs. slip as observed in our simulated dynamic ruptures. We have added the end-member curves for the drained and undrained cases from Viesca and Garagash (2015) to Fig. 9 (new Fig. 11), which exhibit marginal differences on the log-log plot from the solutions of Rice (2006). Both sets of solutions from Viesca & Garagash (2015) and Rice (2006) provide qualitative insight into the increase in  $G$  with slip, but do not provide much detail in the variability for individual points throughout ruptures.

7. Figure 1a. What is the small white triangle? Should this region be shaded blue?

The white section of the dashed red trapezoid in Figure 1a corresponds to the portion of the strain energy change per unit area that corresponds to the breakdown energy outside of the red trapezoid (that arises when the initial and peak shear stress do not coincide). This additional dissipated energy outside of the red trapezoid comes at the expense of the radiated energy. We have added this comment to the caption.

8. Figure 3 and elsewhere. You utilize a 2D model, but then make a comparison to observationally inferred breakdown energy from real earthquakes in 3D. It would be useful to add a few sentences or a paragraph discussing whether or not the 2D idealization alters the predicted scaling behavior. Many people familiar with wave propagation understand that there are substantial differences between 2D and 3D, but for various reasons (discussed, for example, in Freund's Dynamic Fracture Mechanics textbook) this is far less the case for fracture problems. Please comment on this to avoid confusion and to give readers more confidence that the comparison you've made is relevant.

We have added a paragraph in section 5 discussing that the exact scaling relationship between breakdown energy and slip should be examined in 3D simulations. However, the main conclusions of this work that breakdown energy is a rupture-dependent quantity should be the same in 3D models.

9. Figure 5. It appears that there is weakening that is confined to very small slip, prior to the main effects of thermal pressurization. Is this due to the drop in friction coefficient from standard rate-and-state effects? If so, it might be possible to capture this (small) contribution to breakdown energy through a typical LFM fracture energy idealization, as was done by Brantut and Rice (GRL, 2011). Consider commenting on this.

The initial weakening at very small slip in Fig. 5 (new Fig. 6) indeed mostly comes from the drop in friction coefficient due to the standard rate-and-state friction. The dynamic resistance level for the rate-and-state component at 1-10 m/s slip rate would be  $\tau_{ss}(V) = 13.3-13.0$  MPa, comparable to where the rapid drop transitions to more gradual effect due to thermal pressurization, although, for some points, rapid weakening due to adiabatic thermal pressurization seems to start within that small slip as well. It would be difficult to accurately estimate the breakdown energy involved a priori, as we know only the slope of that weakening -  $b \cdot \sigma / D_{rs}$  - but not the peak stress (which depends on the pre-rupture state variable), the very small slips involved, or how much thermal pressurization is mixed in. However, assuming that the thermal pressurization is not yet involved, and taking typical inter-event times 10 years as an estimate for the pre-rupture state variable, we can get the upper bound on the breakdown energy associated with the rate-and-state processes to be  $0.15 \text{ MJ/m}^2$ , much smaller than the overall breakdown energies we obtain. We have added a comment on this to the text.

Referee 2 (E. Tinti)

This paper describes earthquakes rupture histories inferred with dynamic simulations in which thermal pressurization (TP) has a dominant effect. On their dynamic simulations the authors study in particular the breakdown energy considering punctual estimates as well as global/average values. One of the conclusions is that local breakdown energy can exhibit large spatial variations across the fault and large temporal variations on the same location in different earthquake ruptures.

In the literature, dynamic models of real events show heterogeneous distribution of dynamic parameters (usually in terms of initial stress) to reproduce seismological data. I completely agree with the main goal of this paper because the authors try to explain an observed feature (the heterogeneity of dynamic models in space and in time) of real events. The authors compare their theoretical results with estimates coming from real events and find many differences in the scaling relation. I think the study is well designed and the manuscript is clearly written however I have many moderate comments.

Thank you for the positive assessment of our work and comments that helped us improve the manuscript. Please find our responses to your comments below.

My first doubt concerns the definition of breakdown energy. In the literature there is still a confusion about the meaning of fracture energy and I think the authors must do an additional effort to clarify the meaning of this parameter. The shear cracks with the cohesive-zone have been proposed in the literature to overcome the singularity of early crack models and in these model fracture energy is considered as the energy absorbed behind the tip and needed to allow the crack to propagate. In these models, fracture energy surely contains the contribution of surface energy but not heat. In fact, all the dissipations are ascribed to frictional heating (the area below the minimum stress).

Recently in the literature a new definition of fracture energy (as well as the discussion about the meaning of fracture energy on real fault planes) has been proposed to reconcile seismological measurements, geological observations and laboratory experiments and to obtain a coherent understanding of the governing physical processes. Tinti et al (2005) proposed to call “breakdown work” the area below the traction versus slip curve and above the minimum traction value reached when the slip is still increasing (it has been called “work” even if it is an energy, so we can think to it as a breakdown energy). The idea to change the definition and also the symbol ( $W_b$  instead of  $G$ ) was made because all the potential contributions and processes that occur at different length scales during propagation can contribute to this energy: heat, breakage of the asperities as well as comminution of the fault gouge, thermal pressurization, flash heating or other processes absorbed in the fault plane, virtually assumed with an infinitesimal thickness.

For its general definition, this work (or energy) is not constrained to be absorbed just behind the rupture front. The area corresponding to the breakdown work is the only area we are able to “measure” during real events because we cannot know the absolute value of initial stress (it is usually assumed a priori). Because we represent the fault plane as a mathematical virtual plane this area can contain different contribution of energy, also heat.

Looking figure 5 and 7 it seems to me that the authors are generalizing the computation of breakdown energy in the same way. Dynamic models proposed in the literature for real events have to choose a particular data-set of dynamic parameters (e.g.,  $\tau_{yield}$ ,  $\tau_{dyn}$  and  $D_c$  or  $\mu_s$ ,  $\mu_{dyn}$ ,  $\sigma_n$  for SW law, or  $a, b, L$  for R&S law) that fix in some way the breakdown energy of a specific event. The choice of SW law imposes the  $G$  value a priori and does not allow for multiple seismic cycles while the use of R&S law in multiple events allows for a local and temporal variation of  $G$ . I think the study can improve by:

- 1) showing the same figures (5 or 7) for dynamic simulations without TP;
- 2) trying to better explain the meaning of the breakdown energy;
- 3) focusing the interpretation of the results not only on the TP effects but on the difficulties with real events and with current resolution of data to constrain the slip velocity function. More info on this issue are surely useful also for kinematic modelers.

The definition of breakdown energy/work in this study is indeed consistent with that of Tinti et al. (2005). In solid mechanics and engineering, the cohesive-zone models of fracture mechanics have been extensively applied to cracks with all sorts of inelastic processes around the crack tip since 1960s, as long as the inelastic zone is small (small-yield assumption mentioned in the manuscript). In

those cases, the fracture energy  $G$  has already been routinely used to refer to inelastic dissipation broadly, with damage, plastic work, frictional heat etc. often dominating the surface energy. Consider the publication of J. R. Rice, "The Mechanics of Earthquake Rupture", in *Physics of the Earth's Interior* (Proc. International School of Physics 'Enrico Fermi', Course 78, 1979; ed. A. M. Dziewonski and E. Boschi), Italian Physical Society and North-Holland Publ. Co., 1980, pp. 555-649. It stated: "mathematically,  $G$  is the rate (with respect to crack area) of energy loss through the singularity, and physically it is the energy flow to "breakdown" processes at the tip, i.e. the fracture energy" (p. 586), and "microscale cracking processes involved in macroscopic shear faulting will be complex, and will have associated with them a far greater effective fracture energy than for a single tensile crack" (p. 589). The textbook on "Dynamic fracture mechanics" by L. B. Freund uses an example of a cohesive zone calculation based on a (small) plastic zone in front of the crack tip; in that case, physically, most of the associated plastic work that goes into "fracture energy" is actually heat.

We have added a discussion about breakdown energy vs. fracture energy to the introduction.

#### Specific comments

1) Line 17: shear crack or shear pulse (Heaton 1990).

Thank you for the suggestion, we have added it to the text.

2) Line 28: Probably in this sentence the authors would have mentioned Cocco and Tinti 2008 instead of Cocco et al 2004.

We have updated the reference to Tinti et al. (2005) which appears to be the most appropriate reference dedicated to this topic.

2) Figure 1: the authors should explicitly underline that the radiated energy can be computed from the blue area only if the plot represents an average estimate of slip and stress and it is not a punctual plot – as the authors have correctly written in the axes labels (see Kanamori and Rivera 2006).

We have added text emphasizing that the energy balance in Fig. 1 holds for the average stress vs. slip curve for the entire source process, and not the local behavior.

Note that relationship between the energy partitioning, including the radiated energy, and the average stress-slip curve depends on the particular construction of the curve by the averaging of the local evolution stress and slip as discussed in Noda & Lapusta (2012). This is already discussed in section 3 but we have added a more explicit reference to it.

4) Line 45 : "If slip weakening were the fundamental constitutive behavior describing fault resistance during dynamic rupture, then its parameters - the peak resistance, dynamic resistance, and breakdown energy  $G$  - would be expected to be material properties".

I think this sentence is not correct. The authors should say that in literature the SW law is frequently adopted for a single event because it allows to assume (or retrieve) only three parameters ( $\mu_{\text{static}}$  and  $\mu_{\text{dynamic}}$  and  $D_c$ ) and because the slip-weakening behavior has been observed also with R&S law. Often, assuming a SW law simplifies the modeling but it does not mean that the authors believe that  $G$  is a material property as well as  $D_c$ . From laboratory it has been seen that the first two parameters ( $\mu_{\text{static}}$  and  $\mu_{\text{dynamic}}$ ) are material properties even if they also can slightly change due to different conditions of the rock fabric and fault deformation (strain). Differently,  $D_c$  is a debated parameter because it is still not well constrained. So, make the inference that in the literature  $G$  is expected to be a material property is too strong and erroneous.

We agree and we have removed this sentence. The rest of the paragraph in the manuscript already follows the suggested discussion.

We have added text and a figure (Fig. 3) that demonstrate that  $f_{peak}$ ,  $f_{dyn}$ , and  $D_c$  are also not fixed quantities for the standard rate-and state friction.

5) Line 52: “: :and remaining variations in rupture speed are largely controlled by the breakdown energy in such linear slip-weakening representations (Gattereri and Spudich, 2000).” I don’t understand this sentence.

In the direct analogy between breakdown energy and fracture energy for linear slip-weakening friction, the balance between breakdown energy and the released strain energy would be expected to govern the rupture speed. As mentioned in Gattereri and Spudich (2000), the distribution of stress drop and breakdown energy are assumed by seismologists to be the best constrained parameters, under standard slip-weakening descriptions of friction. Static stress drop can be inferred from the final slip distribution and is related to the strain energy released (assuming standard fracture mechanics and ignoring undershoot/overshoot), which allows the breakdown energy to be inferred from variations in rupture speed.

6) Line 55: Many other papers suggest the relation among Breakdown energy and slip (Cocco and Tinti 2008, Brantut and Viesca 2017, Nielsen et al 2016, Selvadurai 2019)

We have added these references as additional evidence for the scaling relationship.

7) Line 56: “which is inconsistent with the breakdown energy being a material property as assumed in linear slip-weakening laws”. I don’t understand: who believes that energy is a property of the materials?

We have altered the term “material property” to “fixed fault property,” which is what we meant to say, and added an explanation in the text. Many in the seismological community have this belief and base their studies on it. For example, some modeling studies have considered faults with assigned heterogeneous  $D_c$  and hence  $G_c$  values, treating them as properties of the interface, and considered sequences of events over such interfaces (e.g., Ide and Aochi, JGR, 2005; Aochi and Ide, 2011). It is also often implicit in ground motion studies that if one can determine the prestress and breakdown energy over the fault, then one may be able to predict the future rupture behavior, as would be the case in a classical linear elastic fracture problem, as already discussed in the conclusions.

8) Line 57: I suggest to add that Perry et al 2020 results have been obtained assuming constant  $L$  parameter on the fault plane.

We have added this in the text.

9) Line 61: Nielsen et al 2016 say that their measures saturate in the rotary lab machine.

We have added text mentioning that qualitatively similar scaling relationships for  $G$  and slip are observed in the lab and that saturation observed by Nielsen et al. (2016).

10) Line 65: Please cite Brantut and Viesca 2017.

We have added this reference in the text.

11) Line 85: Also inferring the dynamic parameters from pseudo-dynamic models (Ide and Takeo 1997, Bouchon et al 1998, Tinti et al 2005, Causse et al 2014) suggest more complex slip weakening behaviors with heterogeneous traction evolutions and heterogeneous dynamic levels.

We have added text mentioning this.

12) Line 88: I don't think the reader can understand the meaning of "Furthermore, the shear heating itself would depend not on the energy counted as "breakdown" but on the overall dissipated energy, making the fault weakening - and hence rupture dynamics - dependent on the absolute stress levels, and not just on stress changes, as typically considered by analogy with traditional fracture mechanics."

We have rephrased this sentence to improve clarity.

13) Why in figure 3 the authors didn't use a more complete dataset?

The values of average simulated breakdown energy, which are compared to the seismological inferences, are from the complete data set for the simulation. In Fig. 4 (old Fig. 3), we include the values of local breakdown energy for locations that experiences a net stress decreases, and hence a clear breakdown of shear stress. This is to illustrate that the continued weakening is thought to translate into both an increase in average and local breakdown energy with increased slip. This is the same simulated data presented in Fig. 11 (old Fig. 9), where we include the points that exhibit a net increase in shear stress (yellow).

As now clarified in the text (section 5), these additional points in Fig 11 (old Fig. 9, in yellow) highlight further conceptual complications in the partitioning of dissipated energy.

14) Lines 95-98: I perfectly agree with this sentence but I would further stress the issue of the slip rate because it's a significant uncertainty of kinematic models.

We have added further illustration and discussion on the variability of slip rate throughout ruptures in the text (e.g. new Fig. 8).

15) Equation (13) is essentially equivalent to equation (1) in Tinti et al 2005 (assuming only one component) or equation (7) in Cocco and Tinti 2008.

This general formulation for the energy associated with the breakdown process was introduced by Palmer & Rice (1973) and Rice (1980) and they have been already cited; we have added the citation to Tinti et al. (2005) as the more recent reference with the same focus. We have added reference to Cocco and Tinti. (2008) in a different portion of the manuscript, with regards to the clarification of breakdown work/energy vs fracture energy.

16) Line 182: I cannot appreciate the meaning because I cannot read Lambert et al in review. But I suppose that also in that case it depends on the assumption of minimum stress level to compute  $G$  during the slip evolution.

Yes, Lambert et al. (in review) explore estimates of average breakdown energy based on dynamic fracture theory for ruptures that exhibit a substantial stress undershoot, such as self-healing pulses. We find that the standard energy balance from the idealized energy diagram (Fig. 1), based on fracture mechanics, does not apply for such ruptures. The Lambert et al. (in review) should be published before this manuscript and we will provide a full citation here.

17) I suggest to change the symbol given to the breakdown energy because it is different to the meaning of fracture energy coming from cohesive-shear cracks.

We would prefer to keep the notation as is. As already discussed in response to an earlier comment, the fracture energy  $G$  of cohesive-shear models has been routinely understood to refer to all types of dissipated energy at the crack/rupture tip, including plastic work, damage, and frictional heat, since at least 1980s. There is an important value in using the notation of  $G$  since it is widely used. We think that it is especially important to continue to use the notation  $G$  as a link to numerous previous works in seismology and to make it widely known that  $G$  almost never relates to only surface energy as

originally thought by Griffith (and erroneously repeated in selected geophysical publications), but rather represents the dissipation (and breakdown, which can also be called fracture) more broadly, even for tensile cracks.

18) How the conditions obtained in a 2D models to arrest the rupture can influence the results respect to a 3D model? How the 2D results have to be scaled to 3D to be compared with estimates from the literature?

We have added a paragraph in section 5 discussing that the exact scaling relationship between breakdown energy and slip should be examined in 3D dynamic rupture simulations, as the spatial distribution of slip and stress evolution differ between 2D and 3D in a nonlinear manner. However, the main conclusions of this work that breakdown energy is a rupture-dependent quantity should be the same in 3D models.

19) Line 225: The authors should underline that the initial stress is the only heterogeneous distribution included in these models and therefore it is the most important parameter that affects the size of the event.

We agree that the prestress before the rupture is the only heterogeneity, other than the VW-VS boundaries, as already discussed in the text. However, emphasizing only the prestress, without recognizing the role of the dynamic stress transfers and the weakening behavior for controlling the size of the rupture, is an oversimplification, as we discuss in the text (section 5). We have included a new figure (Fig. 8) to illustrate. The evolution of shear stress at individual points is due in part from the initial stress and local weakening, as well as the dynamic stress interactions during the rupture process which depend on the initial stress and weakening behavior elsewhere in the rupture. For example, the same prestress distribution would result in different rupture behavior for different efficiency of weakening (Fig. 8). Therefore, it is not enough to know the prestress without knowing the distribution of properties controlling the weakening behavior as well as the dynamic stress redistribution during and throughout the rupture.

20) Figure 7: I would expect a temporal variability of  $G$  for different events because fault properties vary with time (and the equivalent  $\tau_{\text{yield}}$  and  $\tau_{\text{min}}$  are varying during the seismic cycles). The observables up to date seem to give robust information of the average behavior of  $G$  but not on the local estimates. The main problem is that we are not able to infer the slip rate on the fault planes with the actual resolution of seismic data. Results shown in Figure 7 can stress the idea that is very difficult to constrain the local distribution of  $G$  because it can change frequently with time as demonstrated theoretically.

Indeed, this is the motivation for calling  $G$  a rupture-dependent quantity, as it varies at the same location over different ruptures. This is emphasized throughout the text and figures.

21) Figure 6-7: I really like these figures that show how different can be locally the traction evolution as a function of slip due to different slip velocities. I image that the different points on the fault show a very different traction evolution. I suspect that sometime is very difficult to decide which is the minimum traction to fix the area below the curve. Probably there exist many other fault points with heterogeneous slip weakening behavior whose dynamic values reached toward the final slip vary but lies above the first important minimum value, so the area doesn't not increase too much. Moreover, I expect to observe a similar behavior imposing local stress heterogeneities able to produce secondary cracks propagations. I have two comments for these figures:

- (1) I suggest to the authors to discuss about the importance of the knowledge of slip rate more in general and not only linked to TP.
- (2) in figure 7 the authors have selected particular points in which the slip rates have surely two peaks values due to the complexity of the rupture front (as I can see from panels A). Should the authors add a panel with the slip rate function? Central column represents a test case in which  $G$  is more similar

because the rupture front is smoother and slip rate is simpler. This is the reason why in the literature the average estimates of  $G$  are considered more robust than local estimates, both when proposed by spontaneous dynamic models and when calculated on pseudo dynamic models, i.e. constrained by the kinematics of the event.

These are excellent suggestions. We have included a new figure (new Fig. 8) comparing ruptures produced for the same initial stress with and without TP. This demonstrates how TP facilitates rupture propagation under lower prestress, and how local slip rate and stress evolution are highly variable through ruptures. For the R&S friction, the difference in the stress evolution for breakdown is relatively mild, due to the logarithmic dependence on slip rate. This effect is substantially larger in ruptures with TP. Note that the slip rate and stress evolution does not only depend on local prestress but the prestress and weakening conditions throughout the entire rupture through dynamic stress interactions.

22) Probably the reader needs to start from a simpler condition: How is Figure 7 if the authors simulate R&S law with homogeneous parameters, heterogeneous initial stress and without TP?

We have included a new figure (Fig. 8) illustrating the evolution of shear resistance and slip rate in a rupture with only standard rate-and-state friction vs. with TP. We also have added a new figure (Fig. 3) which demonstrates how peak and dynamic friction, as well as slip-weakening distance depend on sliding rate. More detailed examination of the stress evolution and breakdown energy for rate-and-state friction have been shown in a number of previous work, which are referenced along with the new Fig. 3.

23) How is the traction evolution (figure 7) if the authors model an event with R&S law, homogeneous constitutive parameters and constant initial stress with TP (maybe it can be the first modeled event of the seismic cycle)? In this way the reader can appreciate when the effects of TP occur.

We have included a new figure illustrating this (Fig. 8).

24) I suggest to the authors to write that the breakdown energy is the only measurable energy and a future challenge is to understand what does really it represent.

We agree that the physical interpretation of breakdown energy is an open question and a future challenge, and we emphasize this in the conclusions. However, the breakdown energy is a derivative inference and not, as far as we know, a directly measurable quantity. The energy that we hope one can infer seismologically is the radiated energy. The average breakdown energy is then estimated assuming a specific rupture model and relationship between the inferred static stress drop, average slip, radiated energy, and average breakdown energy, as in formula (14) in the manuscript. It is an open question as to whether the local breakdown energy can be reliably inferred, since its relationship to rupture speed is not evident. It is possible that additional constraints can be placed on the total dissipated energy density from thermal arguments, but such constraints would be more of an upper bound, as they would be directly relevant to the specific portion attributed to the breakdown process if the representative residual shear resistance is near zero.

Technical corrections: 1) Line 60: high slip rate ( $>10^3$  m/s) I think there is a mistake or in the number or in the units : : This number is too high if represents m/s.

Yes, there was a typo, the value should be  $10^{-3}$  m/s. We have corrected this in the text.

Literature to add in the references among many other papers:

- 1) Gu and Wong 1991
- 2) Tinti et al 2005. JGR
- 3) Causse et al 2014 GJI

- 4) Nielsen et al 2016: G: Fracture energy, friction and dissipation in earthquakes, J. Seismol,
- 5) Cocco et al 2016, On the scale dependence of earthquake stress drop, J. Seismol.
- 6) Selvadurai, P. A. (2019). JGR
- 7) Brantut and Viesca 2017
- 8) Bizzarri 2010, JGR

We have included most of these references in our manuscript.

**(Interactive comment)**

We would like to kindly call the attention of the authors to some recent literature that appears to be directly relevant to their preprint.

The two recent papers: “The emergence of crack-like behavior of frictional rupture: The origin of stress drops”, Physical Review X 9, 041043 (2019) [<https://doi.org/10.1103/PhysRevX.9.041043>] and “The emergence of crack-like behavior of frictional rupture: Edge singularity and energy balance”, Earth and Planetary Science Letters 531, 115978 (2020) [<https://doi.org/10.1016/j.epsl.2019.115978>] extensively discuss the analogy between frictional rupture and ideal cracks, which is also central to the authors’ preprint.

In particular, the latter paper extensively discusses the relations between the breakdown energy and the edge-localized fracture energy (and the associated length scales). It is found, for generic rate-and-state constitutive relations, that (i) part of the breakdown energy can be identified with a well-defined edge localized fracture energy, which depends on the constitutive relation, that is balanced by the elastic energy flux associated with the edge singularity and that determines the rupture speed. (ii) The breakdown energy can significantly exceed the edge-localized fracture energy, a deviation that is associated with the intrinsic rate-dependence of friction and the lack of strict length scales separation (iii) The breakdown energy is position dependent, even for the very same earthquake rupture propagating along a spatially homogeneous fault.

These findings seem to be directly relevant for the authors’ preprint.

We hope the authors find these comments useful for improving their preprint.

All the very best,

Prof. Eran Bouchbinder, Weizmann Institute of Science, Israel

Prof. Jean-François Molinari, École Polytechnique Fédérale de Lausanne, Switzerland

Dr. Efim Brener, Forschungszentrum Jülich, Germany

Thank you for informing us about this work. The relatively modest variations of breakdown energy in models with standard rate-and-state friction have been examined in several studies already cited in our manuscript (Cocco & Bizzarri, 2002; Rubin & Ampuero, 2005; Ampuero & Rubin, 2008; Lapusta & Liu, 2009; Perry et al., 2020). The suggested work on “The emergence of crack-like behavior of frictional rupture: Edge singularity and energy balance” provides additional insight and hence we added this citation.

# Rupture-dependent breakdown energy in fault models with thermo-hydro-mechanical processes

Valère Lambert<sup>1</sup> and Nadia Lapusta<sup>1,2</sup>

<sup>1</sup>Seismological Laboratory, California Institute of Technology, Pasadena, CA 91125, USA

<sup>2</sup>Department of Mechanical and Civil Engineering, California Institute of Technology, Pasadena, CA 91125, USA

**Correspondence:** Valère Lambert (vlambert@caltech.edu)

**Abstract.** Substantial insight into earthquake source processes has resulted from considering frictional ruptures analogous to cohesive-zone shear cracks from fracture mechanics. This analogy holds for slip-weakening representations of fault friction that encapsulate the resistance to rupture propagation in the form of breakdown energy, analogous to fracture energy, prescribed in advance as if it were a material property of the fault interface. Here, we use numerical models of earthquake sequences with enhanced weakening due to thermal pressurization of pore fluids to show how accounting for thermo-hydro-mechanical processes during dynamic shear ruptures makes breakdown energy rupture-dependent. We find that local breakdown energy is neither a constant material property nor uniquely defined by the amount of slip attained during rupture, but depends on how that slip is achieved through the history of slip rate and dynamic stress changes during the rupture process. As a consequence, the frictional breakdown energy of the same location along the fault can vary significantly in different earthquake ruptures that pass through. These results suggest the need for re-examining the assumption of pre-determined frictional breakdown energy common in dynamic rupture modeling and for better understanding of the factors that control rupture dynamics in the presence of thermo-hydro-mechanical processes.

## 1 Introduction

Fault constitutive relations that describe the evolution of shear resistance with fault motion are critical ingredients of earthquake source modeling. When coupled with the elastodynamic equations of motion, these relations provide insight into the growth and ultimate arrest of ruptures. Earthquake source processes are often considered in the framework of dynamic fracture mechanics, where the earthquake rupture may be considered as a dynamically propagating shear crack or pulse (Ida, 1972; Palmer and Rice, 1973; Madariaga, 1976; Rice, 1980; Kostrov and Das, 1988; Heaton, 1990; Freund, 1990; Kanamori and Heaton, 2000; Rice, 2000; Kanamori and Brodsky, 2004; Rubin and Ampuero, 2005).

20

By analogy to cohesive-zone relations for Mode I opening cracks, slip-weakening laws have been commonly used to describe the dynamic decrease in shear resistance during sliding (Ida, 1972; Palmer and Rice, 1973; Madariaga, 1976; Kostrov and Das, 1988; Kanamori and Brodsky, 2004; Bouchon, 1997; Ide and Takeo, 1997; Olsen et al., 1997; Bouchon et al., 1998; Cruz-Atienza et al., 2009; Kaneko et al., 2017; Gallovic et al., 2019). Linear slip weakening is one of the simplest and most

25 commonly used versions, in which the shear resistance decreases linearly with slip from a peak of  $\tau_{\text{peak}}$  to a constant dynamic level  $\tau_{\text{dyn}}$  achieved at slip of  $D_c$  (Fig. 1).

The breakdown energy  $G$  is associated with the evolution of shear resistance from the initial shear stress  $\tau_{\text{ini}}$  to the peak shear resistance  $\tau_{\text{peak}}$  and then breakdown to the minimum dynamic shear resistance  $\tau_{\text{min}}$ . It is a part of the overall energy partitioning for dynamic ruptures, with the total strain energy change throughout the ruptured region ( $\Delta W$ ) being separated into the radiated energy  $E_R$ , breakdown energy  $G$ , and other residual dissipated energy (Kanamori and Rivera, 2006). The breakdown energy is analogous to fracture energy from cohesive zone models of fracture mechanics (Palmer and Rice, 1973; Rice, 1980; Freund, 1990; Tinti et al., 2005) and hence it is thought to be relevant to rupture dynamics, e.g., rupture speed. For linear slip-weakening friction, it is given by  $G = (\tau_{\text{peak}} - \tau_{\text{dyn}})D_c/2$ . The term "fracture energy," while initially associated with the creation of free surfaces during tensile fracture, has been routinely used to refer broadly to inelastic dissipation relevant to the crack-tip motion for both tensile and shear cracks, including contributions from off-fault damage creation, plastic work, and frictional heat (e.g. Rice, 1980; Freund, 1990; Rice, 2006). However, here we follow the work of Tinti et al. (2005) in referring to this quantity as the "breakdown" work, or energy, to further emphasize that  $G$  can incorporate various physical sources of energy dissipation.

40 More involved fault-constitutive laws are generally required to explain a number of aspects of faulting behavior, most notably the restrengthening of faults in between earthquakes. Laboratory experiments have provided significant insight into the rich behavior of shear resistance, with the frictional response at slip rates between  $10^{-9} - 10^{-3}$  m/s being well-described by rate-and-state friction laws (Dieterich, 2007). A number of previous studies have used models on rate-and-state faults to provide insight into a number of earthquake and slow slip observations, such as sequences of earthquakes on an actual fault segment and repeating earthquakes (Chen and Lapusta, 2009; Barbot et al., 2012; Dieterich, 2007, and references therein). While incorporating a more involved dependence of shear resistance on long-term healing, standard Dieterich-Ruina rate-and-state friction has been shown to resemble linear slip weakening during dynamic rupture (Okubo, 1989; Cocco and Bizzarri, 2002; Lapusta and Liu, 2009), providing further reinforcement of the notion that the breakdown of shear resistance during dynamic rupture may be adequately described by linear slip-weakening behavior.

50 Many studies have attempted to infer parameters of the slip-weakening shear resistance from the strong-motion data resulting from natural earthquakes (Bouchon, 1997; Ide and Takeo, 1997; Olsen et al., 1997; Bouchon et al., 1998; Cruz-Atienza et al., 2009; Kaneko et al., 2017; Galovic et al., 2019). Such studies have noted substantial trade-offs in the inferred parameters during such inversions, such as between the slip-weakening distance  $D_c$  and strength excess  $\tau_{\text{peak}} - \tau_{\text{ini}}$ , where  $\tau_{\text{ini}}$  is the initial stress (Fig. 1). It has been presumed that the spatial distribution of static stress drop and breakdown energy may be the most reliably determined features, as the stress drop can be inferred from the spatial distribution of slip and remaining variations in rupture speed are largely controlled by the breakdown energy in such linear slip-weakening representations (Gattereri and Spudich, 2000).

One of the most notable features of seismologically-inferred breakdown energies from natural earthquakes is that the average breakdown energy from the rupture process has been inferred to increase with the earthquake size (Abercrombie and Rice, 2005; Rice, 2006; Cocco and Tinti, 2008; Viesca and Garagash, 2015; Brantut and Viesca, 2017). Increase in breakdown energy with slip has also been observed in high-speed friction experiments (Nielsen et al., 2016; Selvadurai, 2019), although in some experiments the increase saturates after a given amount of weakening (Nielsen et al., 2016). Such findings are inconsistent with the breakdown energy being a fixed fault property as often assumed in linear slip-weakening laws and as approximately follows from standard rate-and-state friction with uniform characteristic slip-weakening distance (Perry et al., 2020), unless strong and very special heterogeneity is assumed in fault properties. For example, some modeling studies have assigned strongly heterogeneous  $D_c$  and hence  $G$  values to the fault, as if they are properties of the interface, with larger patches having significantly larger values of  $D_c$  and hence  $G$ , and considered sequences of events over such interfaces (e.g. Ide and Aochi, 2005; Aochi and Ide, 2011).

70

Several theoretical and numerical studies have demonstrated that enhanced dynamic weakening, as widely observed at relatively high slip rates ( $> 10^{-3}$  m/s) in laboratory experiments (Tullis, 2007; Di Toro et al., 2011), may explain the inferred increase in breakdown energy with slip (Rice, 2006; Viesca and Garagash, 2015; Brantut and Viesca, 2017; Perry et al., 2020). A number of different mechanisms have been proposed for such enhanced weakening, many of them due to shear heating. For example, thermal pressurization may occur due to the rapid shear heating of pore fluids during slip (Sibson, 1973; Andrews, 2002; Rice, 2006); if pore fluids are heated fast enough and not allowed to diffuse away, they pressurize and reduce the effective normal stress on the fault. Flash heating is another thermally-induced weakening mechanism, where the effective friction coefficient is rapidly reduced due to local melting of highly stressed micro-contacts along the fault (Rice, 1999; Goldsby and Tullis, 2011; Passelegue et al., 2014). Considerations of heat production during dynamic shear ruptures provide a substantial constraint for potential fault models, as field studies show no correlation between faulting and heat flow signatures and rarely suggest the presence of melt (Sibson, 1975; Lachenbruch and Sass, 1980). Models with enhanced weakening have been successful in producing fault operation at low overall prestress and low heat production (Rice, 2006; Noda et al., 2009; Lambert et al., in review) as supported by several observations (Brune et al., 1969; Zoback et al., 1987; Hickman and Zoback, 2004; Williams et al., 2004).

85

Numerical models have shown that the incorporation of thermally-activated enhanced weakening mechanisms during dynamic rupture can have profound effects on the evolution of individual ruptures, as well as the long-term behavior of fault segments, with the potential to make seemingly stable creeping regions fail violently during earthquakes (Noda and Lapusta, 2013), and for the deeper penetration of large ruptures, which may explain the seismic-quietness of mature faults that have historically hosted large earthquakes (Jiang and Lapusta, 2016). Despite evolving dynamic resistance in such models, they can also be consistent with magnitude-invariant static stress drops (Perry et al., 2020).

At the same time, accounting for thermo-hydro-mechanical processes during dynamic rupture can clearly weaken or even remove the analogy between frictional shear ruptures and idealized shear cracks of fracture mechanics. The analogy is based on two key assumptions: 1) that the breakdown of shear resistance is concentrated in a small region near the rupture front, referred to as small-scale yielding, and 2) that there exists a constant residual stress level  $\tau_{\text{dyn}} = \tau_{\text{min}}$  throughout the ruptured region during sliding (Palmer and Rice, 1973; Freund, 1990). **For example, the relationship between rupture speed and fracture energy of linear elastic fracture mechanics is on valid under these assumptions.** Clearly, these assumptions can become invalid when thermo-hydro-mechanical processes are considered. For example, shear heating can raise the pore fluid pressure in regions away from the rupture front and weaken the fault there, contributing to the breakdown of fault resistance away from the rupture tip and varying the dynamic resistance level. Furthermore, the shear heating itself would **depend on the overall dissipated energy, making the fault weakening behavior, and hence "breakdown," depend on the absolute stress levels, and not just the stress changes, as typically considered by analogy with traditional fracture mechanics. Moreover, studies that infer dynamic parameters from natural earthquakes using dynamically-inspired kinematic models suggest more complicated evolutions of shear stress with slip, including heterogeneous dynamic resistance levels (Ide and Takeo, 1997; Bouchon et al., 1998; Tinti et al., 2005; Causse et al., 2013)**

**In this study,** we use numerical models of earthquake sequences with enhanced weakening due to thermal pressurization to illustrate how the inclusion of thermo-hydro-mechanical processes during dynamic shear ruptures makes breakdown energy rupture-dependent, in that the value of both local and average breakdown energy vary among ruptures on the same fault, **even with spatially uniform and time-independent** constitutive properties. As such, the breakdown energy is not an intrinsic fault property, but **develops** different values at a given location, depending on the details of the rupture process, which in part depend on the prestress before the dynamic rupture achieved as a consequence of prior fault slip history. Moreover, the local breakdown energy is not uniquely defined by the amount of slip attained during rupture, but depends on how that slip was achieved through the complicated history of slip rate and dynamic stress changes throughout the rupture process. **Additional fault characteristics that we do not consider here, such as heterogeneity in fault properties and dynamically-induced, evolving, inelastic off-fault damage (Dunham et al., 2011a, b; Roten et al., 2017; Withers et al., 2018) should result in qualitatively similar effects and add even more variability to the breakdown energy.**

## 2 Description of numerical models

We conduct numerical simulations of spontaneous sequences of earthquakes and aseismic slip (SEAS) utilizing the spectral boundary integral method to solve the elastodynamic equations of motion coupled with friction boundary conditions, including the evolution of pore fluid pressure and temperature on the fault coupled with off-fault diffusion (Lapusta et al., 2000; Noda and Lapusta, 2010). Our simulations consider mode III slip on a 1-D fault embedded into a 2-D uniform, isotropic, elastic medium slowly loaded with a long-term slip rate  $V_{pl}$  (Fig. 2). The simulations resolve the full slip behavior throughout earthquake sequences, including the nucleation process, the propagation of individual dynamic ruptures, as well as periods of post-seismic

and the interseismic slip between events that can last for months to hundreds of years.

Our fault models adopt the laboratory-derived Dieterich-Ruina rate-and-state friction law with the state evolution governed by the aging law (Dieterich, 1979; Ruina, 1983):

$$130 \quad \tau = \bar{\sigma} f(V, \theta) = (\sigma - p) \left[ f_* + a \log \frac{V}{V_*} + b \log \frac{\theta V_*}{D_{RS}} \right], \quad (1)$$

$$\dot{\theta} = 1 - \frac{V\theta}{D_{RS}}, \quad (2)$$

where  $\bar{\sigma}$  is the effective normal stress,  $\sigma$  is the normal stress,  $p$  is the pore fluid pressure,  $f_*$  is the reference steady-state friction coefficient at reference sliding rate  $V_*$ ,  $D_{RS}$  is the characteristic slip distance, and  $a$  and  $b$  are the direct effect and evolution effect parameters, respectively. Other formulations for the evolution of the state variable exist, such as the slip law (Ruina, 1983) as well as various composite laws, and the formulation that best describes various laboratory experiments remains a topic of ongoing research (Bhattacharya et al., 2015, 2017; Shreedharan et al., 2019). However, the choice of the state evolution law should not substantially influence the results of this study, as the evolution of shear resistance during dynamic rupture within our simulations is dominated by the presence of enhanced weakening mechanisms. We use the version of the expressions (1) and (2) regularized for zero and negative slip rates (Noda and Lapusta, 2010).

140 During conditions of steady-state sliding ( $\dot{\theta} = 0$ ), the friction coefficient is expressed as:

$$f_{ss}(V) = f_* + (a - b) \log \frac{V}{V_*}. \quad (3)$$

The combination of frictional properties  $(a - b) > 0$  results in steady-state velocity-strengthening (VS) behavior, where stable slip is expected, and properties resulting in  $(a - b) < 0$  lead to steady-state velocity-weakening (VW) behavior, where accelerating slip and hence stick-slip occur for sufficiently large regions (Rice and Ruina, 1983; Rice et al., 2001; Rubín and Ampuero, 2005).

An important, yet often underappreciated, implication of the rate- and state-dependent effects observed in laboratory experiments is that notions of static and dynamic friction coefficients, as well as the slip-weakening distance, are not well-defined and fixed quantities, as would be considered by standard linear slip-weakening laws (Cocco and Bizzarri, 2002; Rubín and Ampuero, 2005; Ampuero and Rubín, 2008; Lapusta and Liu, 2009; Barras et al., 2019; Perry et al., 2020). Instead, they depend on the history and current style of motion. For example, the dynamic friction, comparable to the steady-state friction at dynamic slip rates, depends on slip rate (Eq. 3), which can vary substantially throughout rupture and between different ruptures. Moreover, the peak friction and effective slip-weakening distance under standard rate-and-state friction depend on the history of motion through the state variable  $\theta$ , as well as the sliding rate during fast slip (Fig. 3). Let us consider a point with the same initial friction but different periods of inter-event healing, captured by increasingly larger values of the pre-rupture state variable. If the point is now driven to slide at a fixed sliding rate, the peak friction and slip-weakening distance would be larger for points that (i) have higher pre-rupture value of the state variable, representing better healed interfaces, and/or (ii) sliding at

160 faster slip rates (Fig. 3). For standard rate-and-state friction, these effects typically translate into generally mild variations in dynamic/static stress drop and breakdown energy, due to the logarithmic dependence of the shear stress evolution on slip rate, resulting in both static stress drop and breakdown energy being effectively rupture-independent (Cocco and Bizzarri, 2002; Rubin and Ampuero, 2005; Ampuero and Rubin, 2008; Lapusta and Liu, 2009; Perry et al., 2020), at least compared to the large variations of breakdown energy with slip inferred from natural earthquakes as discussed in the introduction. However, such variations in stress evolution become more substantial with enhanced dynamic weakening mechanisms that lead to stronger rate-dependent weakening.

170 Laboratory experiments indicate that the standard rate-and-state laws (Eqs. 1 - 2) provide good descriptions of frictional behavior at relatively slow slip rates ( $10^{-9}$  to  $10^{-3}$  m/s). However, at higher sliding rates, including average seismic slip rates of  $\sim 1$  m/s, additional enhanced weakening mechanisms can occur, such as the thermal pressurization of pore fluids. Thermal pressurization is governed in our simulations by the following coupled differential equations for the evolution of temperature and pore fluid pressure (Noda and Lapusta, 2010):

$$\frac{\partial T(y, z; t)}{\partial t} = \alpha_{\text{th}} \frac{\partial^2 T(y, z; t)}{\partial y^2} + \frac{\tau(z; t)V(z; t)}{\rho c} \frac{\exp(-y^2/2w^2)}{\sqrt{2\pi}w}, \quad (4)$$

$$\frac{\partial p(y, z; t)}{\partial t} = \alpha_{\text{hy}} \frac{\partial^2 p(y, z; t)}{\partial y^2} + \Lambda \frac{\partial T(y, z; t)}{\partial t}, \quad (5)$$

175 where  $T$  is the pore fluid temperature,  $\alpha_{\text{th}}$  is the thermal diffusivity,  $\tau V$  is the shear heating source which is distributed over a Gaussian shear layer of half-width  $w$ ,  $\rho c$  is the specific heat,  $y$  is the fault-normal distance,  $\alpha_{\text{hy}}$  is the hydraulic diffusivity, and  $\Lambda$  is the coupling coefficient that provides the change in pore pressure per unit temperature change under undrained conditions.

180 The total fault domain of size  $\lambda$  is partitioned into a frictional region of size  $\lambda_{\text{fr}}$  where we solve for the balance of shear stress and frictional resistance, as well as loading regions at the edges where the fault is prescribed to slip at a tectonic plate rate (Fig. 2A). The frictional interface is composed of a 24-km region with VW frictional properties of size  $\lambda_{\text{VW}}$ , surrounded by a velocity-strengthening domain. The majority of the seismic events arrest within the VW region, which we refer to as "partial ruptures," however some span the entire VW region, which we refer to as "complete ruptures" (Fig. 2C). **Weakening due to thermal pressurization is confined to the region with the VW properties.** The parameter values used for the simulations presented in this work are motivated by prior studies (Rice, 2006; Noda and Lapusta, 2010; Perry et al., 2020) and provided in 185 Table 1.

### 3 Energy partitioning and notion of breakdown energy $G$

In the earthquake energy budget, the total strain energy change per unit source area  $\Delta W/A$  is partitioned into the dissipated energy per unit area,  $E_{\text{Diss}}/A$ , and the radiated energy per unit area,  $E_R/A$ :

$$\Delta W/A = E_{\text{Diss}}/A + E_R/A. \quad (6)$$

190 The total strain energy released per unit area  $\Delta W/A$  is given by:

$$\Delta W/A = \frac{1}{2}(\bar{\tau}_{\text{ini}} + \bar{\tau}_{\text{fin}})\bar{\delta}, \quad (7)$$

where  $\bar{\delta}$  is the average final slip for the event, and  $\bar{\tau}_{\text{ini}}$  and  $\bar{\tau}_{\text{fin}}$  are the average initial and final shear stress weighted by the final slip (Noda and Lapusta, 2012), respectively,

$$\bar{\tau}_{\text{ini}} = \frac{\int_{\Omega} \tau_{\text{ini}}(z) \delta_{\text{fin}}(z) dz}{\int_{\Omega} \delta_{\text{fin}}(z) dz}, \quad (8)$$

$$195 \quad \bar{\tau}_{\text{fin}} = \frac{\int_{\Omega} \tau_{\text{fin}}(z) \delta_{\text{fin}}(z) dz}{\int_{\Omega} \delta_{\text{fin}}(z) dz}. \quad (9)$$

Here,  $\Omega$  represents the ruptured domain. The static stress drop is a measure of the difference in average stress before and after the rupture. The relevant definition of average static stress drop for energy considerations is the energy-based or slip-weighted stress drop (Noda et al., 2013):

$$\overline{\Delta\tau} = \bar{\tau}_{\text{ini}} - \bar{\tau}_{\text{fin}} = \frac{\int_{\Omega} [\tau_{\text{ini}}(z) - \tau_{\text{fin}}(z)] \delta_{\text{fin}}(z) dz}{\int_{\Omega} \delta_{\text{fin}}(z) dz}. \quad (10)$$

200 The dissipated energy per unit rupture area can be computed from the evolution of shear resistance with slip:

$$E_{\text{Diss}}/A = \frac{\int_{\Omega} \left[ \int_0^{\delta_{\text{fin}}(z)} \tau(\delta') d\delta' \right] dz}{\int_{\Omega} dz}. \quad (11)$$

The dissipated energy  $E_{\text{Diss}}/A$  is often further partitioned into the average breakdown energy  $G$  (Palmer and Rice, 1973; Rice, 1980; Tinti et al., 2005) and residual dissipated energy (dark grey triangle and light grey rectangle in Fig. 1, respectively). The average breakdown energy represents the spatial average of the local breakdown energy  $G_{\text{loc}}$  within the source region,

$$205 \quad G = \frac{\int_{\Omega} G_{\text{loc}}(z) dz}{\int_{\Omega} dz} \quad (12)$$

where the local breakdown energy is defined as,

$$G_{\text{loc}}(z) = \int_0^{D_c(z)} [\tau(\delta') - \tau_{\text{min}}(z)] d\delta', \quad (13)$$

and  $\tau_{\text{min}}(z)$  is the minimum local shear resistance during seismic slip after the initial strengthening from the initial to peak shear resistance via the direct effect.  $D_c$  is defined as the critical slip distance during the rupture such that  $\tau(D_c(z)) = \tau_{\text{min}}(z)$ .

210

Seismological studies have attempted to estimate the average breakdown energy for natural earthquakes based on the standard energy partitioning diagram (Fig. 1) as follows (Abercrombie and Rice, 2005; Rice, 2006):

$$G' = \frac{\bar{\delta}}{2} \left( \overline{\Delta\tau} - \frac{2\mu E_R}{M_0} \right), \quad (14)$$

where  $G'$  is the approximation for the average breakdown energy  $G$ ,  $\bar{\delta}$  is the average slip during the rupture,  $\overline{\Delta\tau}$  is the  
215 seismologically-inferred average static stress drop,  $\mu$  is the shear modulus,  $E_R$  is the radiated energy and  $M_0$  is the seismic  
moment. The definition of  $G'$  assumes that the rupture area exhibits negligible stress overshoot/undershoot, or that the average  
level of dynamic resistance during sliding is the same as the final average shear stress. Numerical studies have shown that  $G'$   
may indeed provide a reasonable estimate of the average breakdown energy (within a factor of 2) for crack-like ruptures, which  
exhibit mild overshoot/undershoot compared to the static stress drop (Perry et al., 2020), however such estimates can dramati-  
220 cally differ from the true values for ruptures that experience a considerable stress undershoot, as is the case of self-healing  
pulse-like ruptures (Lambert et al., in review).

Note that the energy balance shown in Eq. 6 reflects the energy partitioning over the rupture process as a whole. While the  
dissipated energy is a local quantity along the fault, the radiated energy is not and can only be related to the stress-slip behavior  
225 in the averaged sense over the entire rupture process (Fig. 1). Seismological estimates of the average breakdown energy can  
be made assuming the standard energy partitioning following the slip-weakening diagram (Fig. 1) and using Eq. 14 with the  
total radiated energy, with the results dependent on the accuracy of the radiated energy estimates and validity of the assumed  
energy partitioning model, which has been shown to breakdown for pulse-like ruptures (Lambert et al., in review). Estimating  
the local breakdown energy is more challenging. One approach is to use finite-fault slip inversions to determine the stress  
230 evolution during rupture and hence the breakdown work (e.g. Tinti et al., 2005), with the results dependent on the accuracy of  
finite-fault inversions that are known to be non-unique and affected by smoothing.

#### 4 Breakdown energy in models with thermal pressurization of pore fluids

The local slip and stress evolution are determined at every point along the fault within our simulations at all times, thus we  
can calculate the local dissipation and breakdown energy throughout each rupture as well as study these quantities evolve in  
235 different ruptures throughout the sequence. We can also compute the average energy quantities and construct the average stress  
vs. slip curves for the total rupture process in a manner that preserves the overall energy partitioning (Noda and Lapusta, 2012).  
We define seismic slip to occur when the local slip velocity exceeds a velocity threshold  $V_{\text{thresh}} = 0.01$  m/s. As slip rates during  
sliding are typically around 1 m/s or higher and drop off rapidly during the arrest of slip, modest changes of this velocity  
threshold by an order of magnitude produce very mild differences in  $D_c$  and  $G$ , by less than 1%.

240

The average breakdown energy  $G$  computed from our simulations increase with average slip and matches estimates of  
breakdown energy for natural events (Fig. 4), as expected from the simplified theoretical considerations (Rice, 2006). As  
demonstrated in previous numerical studies (Perry et al., 2020), when our fault models combine moderately efficient thermal  
pressurization with persistently weak conditions, such as from relatively low interseismic effective normal stresses (25 MPa)  
245 due to substantial chronic fluid overpressurization, the models produce mostly crack-like ruptures that reproduce all main ob-  
servations about earthquakes, including magnitude-invariant average static stress drops of 1-10 MPa, breakdown energy values

that are quantitatively comparable to estimates from natural earthquakes, and fault temperatures well below representative equilibrium melting temperatures near 1000° C for wet granitic compositions in the shallow crust (Rice, 2006). It is important to note that the presence of enhanced dynamic weakening is critical for producing reasonable values of static stress drop (> 1  
250 MPa) in such fault models with chronic fluid overpressurization; otherwise, the stress changes due to the standard rate-and-state friction would be too low (as they are proportional to the effective normal stress). As such, dynamic weakening due to thermal pressurization still dominates the overall weakening behavior during dynamic rupture. These results suggest that fault models incorporating chronic fault weakness and enhanced weakening may be plausible representations of rupture behavior on mature faults. The work of Perry et al. (2020) and Lambert et al. (in review) provide a broader exploration of models with different  
255 parameters, including different levels of interseismic effective stresses and efficiency of enhanced dynamic weakening. Here, we use a representative model to illustrate the resulting properties of the breakdown energy in such models.

Let us examine the spatial distribution of shear stress and breakdown energy in three ruptures of varying size within the same simulated sequence of earthquakes (Fig. 5). All three ruptures nucleate, propagate, and arrest predominantly in the VW region  
260 that has uniform fault properties, the only difference being how big the events become. The distribution of shear stress along the fault before each rupture is heterogeneous due to the stress drop from previous ruptures. While each earthquake nucleates in a region with approximately the same locally-high initial stress, the ruptures propagate and arrest over regions with lower prestress. Larger ruptures with more slip experience greater weakening and larger local stress drops in some regions, which facilitates further rupture propagation over areas of lower prestress. As such, while the final average shear stress decreases for  
265 larger ruptures, the average initial stress also decreases, resulting in nearly magnitude-invariant average stress drops.

Despite the fault constitutive properties being uniform and constant in time, the breakdown energy varies spatially within each event as well as differs at each location for different ruptures (Figs. 5C and 6). Larger ruptures that experience larger average slip also exhibit more weakening, resulting in the average breakdown energy generally increasing with the rupture  
270 size (Fig. 5C). If we examine individual points that are common among all three ruptures, we see that the local breakdown energy also varies as the points experiences different degrees of slip and overall weakening behavior (Fig. 6). This suggests that the local and average breakdown energy is not just a function of the local fault material properties, but a more complicated evolution of effective weakening behavior and stress throughout the rupture.

275 Note that the breakdown energy illustrated in Fig. 6 is dominated by the thermal pressurization of pore fluids, with negligible contribution from the weakening due to standard rate-and-state friction. The breakdown energy due to rate-and-state friction can be estimated as (Perry et al., 2020):

$$G = \frac{1}{2} b \bar{\sigma} D_{RS} \left( \log \frac{\theta_{ini} V_{dyn}}{D_{RS}} \right)^2 \quad (15)$$

where the effective normal stress  $\bar{\sigma}$  is assumed to be constant,  $\theta_{ini}$  is the value of the state variable at the beginning of slip,  
280 and  $V_{dyn}$  is the representative dynamic slip rate. Assuming that  $\bar{\sigma}$  is still approximately given by the interseismic value at the

beginning of slip (which would produce an upper bound),  $\theta_{\text{ini}}$  is given by the representative inter-event time of 10 years, and  $V_{\text{dyn}}$  is given by the representative peak rate of 10 m/s, the breakdown energy due to the standard rate-and-state friction in our simulation has the upper bound of 0.15 MJ/m<sup>2</sup>. This is an order of magnitude smaller than the values of 1 to 6 MJ/m<sup>2</sup> of Fig. 6.

## 285 5 Overall increase of breakdown energy with slip and significant rupture-dependent scatter

Previous theoretical work has demonstrated how the incorporation of thermo-hydro-mechanical processes such as the thermal pressurization of pore fluids can explain the inferred increase in breakdown energy with increasing event size (Rice, 2006). The work of Rice (2006) presented solutions for two end-member cases for the evolution of shear resistance and breakdown energy with thermal pressurization, illustrating how continuous weakening occurs with slip and results in breakdown energy  
290 increasing with slip.

If slip occurs within a layer of thickness  $h$  that is large enough to justify the neglect of heat and fluid transport, conditions may be considered adiabatic and undrained, which may be relevant for relatively short slip durations (Rice, 2006; Viesca and Garagash, 2015). Under such conditions, the weakening behavior is controlled by the ratio of the coupling coefficient  $\Lambda$  and  
295 specific heat  $\rho c$ , as well as the thickness of the shearing layer  $h$  which controls the efficiency of heat production. Assuming a constant friction coefficient  $f$  and slip rate  $V$ , one can express the evolution of shear resistance  $\tau$  and breakdown energy  $G$  as functions of slip (Rice, 2006),

$$\tau(\delta) = f(\sigma - p_0) \exp\left(-\frac{f\Lambda}{\rho c} \frac{\delta}{h}\right), \quad (16)$$

$$G(\delta) = \frac{\rho c(\sigma - p_0)h}{\Lambda} \left[1 - \left(1 + \frac{f\Lambda\delta}{\rho ch}\right) \exp\left(-\frac{f\Lambda\delta}{\rho ch}\right)\right]. \quad (17)$$

300 Under such conditions, increasing slip results in continued weakening of the shear resistance and increasing values of breakdown energy. The continued weakening is the result of shear heating and subsequent pressurization, which remains active as long as the slip rate and shear stress are non-zero.

The inclusion of thermal and hydraulic diffusion introduces a diffusion time-scale to the problem, which governs the efficiency of weakening over extended slip durations. If one considers slip on a mathematical plane, a characteristic weakening  
305 time-scale  $t^*$ , may be defined assuming a constant friction coefficient and slip rate (Mase and Smith, 1987):

$$t^* = \frac{4}{f^2} \left(\frac{\rho c}{\Lambda}\right)^2 \frac{(\sqrt{\alpha_{\text{hy}}} + \sqrt{\alpha_{\text{th}}})^2}{V^2}. \quad (18)$$

Rice (2006) demonstrated that this may be related to a characteristic slip-weakening distance for thermal pressurization,

$$L^* = \frac{4}{f^2} \left(\frac{\rho c}{\Lambda}\right)^2 \frac{(\sqrt{\alpha_{\text{hy}}} + \sqrt{\alpha_{\text{th}}})^2}{V}, \quad (19)$$

310 such that the evolution of shear resistance and breakdown energy for slip on a plane may also be expressed as a function of slip (Rice, 2006):

$$\tau(\delta) = f(\sigma - p_0) \exp\left(\frac{\delta}{L^*}\right) \operatorname{erfc}\left(\sqrt{\frac{\delta}{L^*}}\right), \quad (20)$$

$$G(\delta) = f(\sigma - p_0) L^* \left[ \exp\left(\frac{\delta}{L^*}\right) \operatorname{erfc}\left(\sqrt{\frac{\delta}{L^*}}\right) \left(1 - \frac{\delta}{L^*}\right) - 1 + 2\sqrt{\frac{\delta}{\pi L^*}} \right]. \quad (21)$$

315 Unlike the case of a critical slip-weakening distance  $D_c$  in standard slip-weakening models, the weakening of shear resistance is continuous with increasing slip (Fig. 7a), with  $L^*$  providing a measure of how much slip is needed to weaken by a certain degree. Note that the evolution of stress in Eqs. (16) and (20) do not consider the elastic interactions that occur due to non-uniform slip within finite ruptures, and therefore assume that the slip velocity is not only temporally constant, but spatially uniform over the fault.

320 Both of these thermal pressurization solutions have the convenient feature of expressing the breakdown of shear resistance as a function of slip, drawing familiarity to standard slip-weakening notions of shear fracture. As pointed out by Rice (2006), the representation of breakdown energy purely as a function of slip is a considerable simplification, whereas the physics underlying the mechanisms for weakening require that  $\tau$  is a complicated function of the slip rate history up to the current time. During dynamic rupture, the local slip rate experiences considerable acceleration near the rupture front, resulting in a more pronounced weakening rate (Fig. 7), which in turn facilitates large dynamic stresses and higher slip rates in other parts of the rupture. As the rupture front passes, both the slip rate and weakening rate decrease. However, the slip rate may persist around typical seismic values of 1 m/s until the arrival of arrest waves from the edges of the rupture or local healing. Note that while the slip rates behind the rupture front in our models appear more or less stable around 1 m/s (Fig. 7E and G), they may vary depending on the arrival of wave-mediated dynamic stresses from other slipping regions in the rupture, which drive prolonged slip and therefore modulate the weakening rate due to shear heating mechanisms like thermal pressurization. In general, the friction coefficient may also vary considerably with the slip rate, particularly when accounting for additional enhanced weakening processes such as flash heating (Rice, 1999; Goldsby and Tullis, 2011; Passelegue et al., 2014).

335 The continued weakening with slip due to thermal pressurization is an important factor that drives rupture propagation and allows ruptures to propagate under lower, and hence less favorable, prestress conditions. Let us consider two fault models with the same initial prestress and the same rate-and-state frictional parameters, but with and without enhanced weakening due to thermal pressurization (Fig. 8). The rupture governed by only standard rate-and-state friction exhibits relatively mild stress variations with slip rate and thus requires higher prestress conditions to propagate. While the local slip rate evolution varies among points throughout the rupture, the evolution of shear resistance with slip associated with the breakdown process is generally comparable throughout the rupture with uniform rate-and-state properties (Fig. 8 left column). In contrast, the rupture that is driven by enhanced weakening due to thermal pressurization experiences a stronger feedback between the evolution of shear stress and slip rate, resulting in a much larger rupture that propagates over lower prestress conditions. The evolution of

slip rate is highly variable for different points throughout the crack-like rupture, with long tails of seismic slip behind the rupture front that experience periods of acceleration and deceleration due to dynamic stress interactions from neighboring points.

345 This variability in local slip rate translates into further variability in local weakening, even for points with the same initial prestress. This emphasizes that the local weakening behavior, and the associated breakdown energy, depend not only on the local prestress and weakening properties, but also the distribution of prestress and weakening behavior throughout the entire rupture process.

350 An important consequence of continued fault weakening is that much of the additional dissipated energy, which leads to the increase of breakdown energy with continued slip, is not concentrated near the rupture front (Fig. 7). Moreover, weakening may not actually be strictly monotonic but local points can experience transient increases in shear stress as they begin to arrest, but then are loaded by neighboring slipping regions and forced to slip and weaken further (Fig. 6 and 10). The continued and variable weakening of shear resistance behind the rupture front emphasizes a critical difference between dynamic shear rup-

355 tures and mode I fracture, where the crack surface is typically traction-free behind the cohesive zone at the rupture front. The attribution of the continually dissipated energy to the breakdown process governing rupture propagation is also inconsistent with the assumption of small-scale yielding, which facilitated the original mathematical analogy based on laboratory constitutive relations derived at lower slip-rates (Palmer and Rice, 1973).

360 While breakdown energy does not appear to be a constant material property, one may ask if the effects of local weakening due to thermal pressurization may be adequately encapsulated into a slip-weakening formulation such as Eqs. (16-20). To gain insight into such possibility, let us examine three large ruptures in our simulations that have comparable average slip and breakdown energy (Fig. 9). If we consider the evolution of local shear stress and slip at points shared among the three ruptures, we can see that the local breakdown energy differs even for comparable local slip. Moreover, the three points, which share the

365 same constitutive description, do not exhibit a systematic scaling relationship between local slip and breakdown energy. For example, the point at  $z = -4.8$  km exhibits a generally increasing trend in local  $G$  with increasing slip, whereas the point at  $z = 4.8$  km shows decreasing values of  $G$  for increasing slip among the three ruptures (Fig. 9C vs. E). The point in the center of the rupture ( $z = 0$ ) does not even exhibit a monotonic trend, as  $G$  both increases and decreases for ruptures with increasing slip (Fig. 9D). Indeed, if we examine the spatial distribution of local stress and breakdown energy within each rupture, we see

370 that while the three ruptures have comparable average  $G$  and slip, they achieve both in different ways (Fig. 10).

The general trend of increasing breakdown energy with slip qualitatively holds for most local points within our simulated ruptures, however there is considerable variability for individual values of  $G$  at a given slip (Fig. 11). While values of average breakdown energy and slip for individual ruptures appear to demonstrate a consistent scaling relationship, these average values

375 smooth out the greater variability in local breakdown energy and slip. For points within our simulated ruptures that experience a net decrease, or **breakdown**, in shear stress, the local  $G$  is generally within a factor of 3 of the scaling relationship between average  $G$  and average slip. This variation adds up to approximately an order of magnitude variation in local  $G$  for some values

of slip.

380 For frictional ruptures, substantial slip may occur in regions that experience a net increase in shear stress, particularly in the regions near the **rupture** arrest (Fig. 6B). We find that points in our simulated ruptures that experience a net increase in shear stress exhibit greater variability in  $G$  with slip (Fig. 11, yellow circles), potentially due to the greater variability in slip rate during rupture deceleration and arrest. **These points illustrate the challenge of partitioning the dissipated energy into components that are thought to be, and not be, relevant to the dynamic rupture process. These points exhibit no net local breakdown**  
385 **of shear resistance but rather a net strengthening. A more appropriate approach may be to distinguish between concepts of breakdown energy and "restrengthening energy," as discussed in Tinti et al. (2005). However, the physical relevance for either component, or their distinction, during the rupture process is not directly evident. Understanding the physical significance of different components of dissipated energy for dynamic rupture propagation is an important topic of active research.**

390 The theoretical considerations of Rice (2006) have been extended to the spatially and temporally variable slip rate associated with steady rupture propagation (Viesca and Garagash, 2015). Approximate expressions for the scaling of breakdown energy with slip can be presented for end-member conditions of undrained  $G_u(\delta)$  and drained  $G_d(\delta)$  weakening as:

$$G_u(\delta) \approx f(\sigma - p_0) \frac{f\Lambda\delta^2}{2\rho ch}, \quad \text{undrained, small slip} \quad (22)$$

395  $G_d(\delta) \approx (12\pi)^{-1/3} f(\sigma - p_0) L^{*1/3} \delta^{2/3}, \quad \text{slip on a plane, large slip.} \quad (23)$

Similar to the solutions (17) and (21) that assume constant slip rate, the steady-state solutions (22-23) do not capture the variability of the local breakdown energy with slip seen in our simulated dynamic ruptures (Fig. 11). This is because our simulated dynamic ruptures do not exhibit steady rupture propagation, but rather have considerable spatial variations in slip rate evolution, as likely the case for natural earthquake ruptures. This comparison illustrates a limitation of steady-state rupture  
400 solutions for examining rupture properties that are highly sensitive to spatial heterogeneity in slip motion, such as breakdown energy in the presence of thermal pressurization.

While the general increase in breakdown energy with slip is qualitatively consistent among the theoretical solutions and our simulated dynamic ruptures in 2D models with 1D faults (Fig. 11), the scaling relationship between breakdown energy and slip  
405 would be best studied in 3D models of dynamic rupture with 2D faults. For example, for ruptures on 2D faults would have a larger fraction of the ruptured area associated with rupture arrest and hence may demonstrate a wider scatter in local  $G$ , as seen by points in our simulated ruptures that experience a net increase in shear stress. In addition, it would be prudent to examine any differences in scaling behavior for ruptures that are geometrically confined along a given direction, as may be representative of large crustal earthquakes. However, we expect that the main results of this work - that the local and average breakdown energy  
410 can vary among ruptures and are not unique functions of slip - would be consistent with 2D rupture scenarios in 3D models.

## 6 Conclusions

The average breakdown energy for our simulated ruptures tends to increase with increasing rupture size and average slip in a manner consistent with inferences from field observations and simplified theoretical models (Rice, 2006; Viesca and Garagash, 2015). At the same time, the values of local breakdown energy for a given amount of slip have a wide spread in our  
415 simulations, even though the constitutive properties are uniform and **time-independent** along the fault, highlighting the reality that breakdown energy in models with thermo-hydro-mechanical mechanisms is not fundamentally a function of slip. In fact, ruptures with near-uniform slip can have local values of the breakdown energy vary by as much as a factor of 4 (Fig. 10C), making a homogeneous fault appear to be heterogeneous. This is because the breakdown energy depends on the specific history of motion and dynamic stress changes that occur throughout individual rupture processes. Furthermore, since the history of  
420 rupture motion is determined, in part, by the fault prestress before the dynamic rupture, the breakdown energy also depends on the history of other slip events on the fault that determine the prestress.

The analytic formulations for the evolution of shear resistance with slip for the thermal pressurization presented by Rice (2006) provide profound insight into the first-order behavior of such thermally-activated hydro-mechanical weakening mech-  
425 anisms. However, they are based on the kinematic assumptions of a *spatially uniform and temporally constant* slip velocity, as well as a constant friction coefficient, that allow for the weakening rate to be determined as a function of slip. In the fully dynamic statement of the problem, the evolving and spatially non-uniform slip rate is a key part of the solution which leads to the evolution in the associated shear heating and weakening/strengthening of the fault that depend not only on the amount of slip but also on how that slip is achieved through the complex history of slip velocity. **Our results demonstrate that the  
430 extension to steady-state rupture solutions with non-constant slip rate (Viesca and Garagash, 2015) similarly does not capture the variability in local breakdown energy associated with the complex and evolving history of slip velocity and dynamic stress interactions in non-steady ruptures, even in fault models with uniform fault properties like ours.**

Note that this variability in local  $G$  for a given slip is achieved among points with uniform and constant constitutive prop-  
435 erties. Such variability in the effective weakening rate and  $G$  may become more pronounced in the presence of fault heterogeneity, such as for geometrically rough faults with variable effective normal stress, or if the hydraulic properties of the shearing layer and surrounding rock were to evolve during the rupture process, such as from changes in rock permeability due to off-fault damage. The evolution of permeability during dynamic rupture may have considerable implications for the role of thermo-hydro-mechanical processes in the evolution of shear resistance on faults and it is an important topic for future work.

440

While we follow the assumption that most of the breakdown energy occurs on the shearing surface (Rice, 2006; Viesca and Garagash, 2015), additional dissipation may also come from the production of damage and off-fault inelastic deformation (Poliakov et al., 2002; Andrews, 2005; Okubo et al., 2019), especially on rough, non-planar faults (Dunham et al., 2011b). Such sources of additional dissipated energy may contribute to the inferred increase in average breakdown energy with average slip

445 for natural earthquakes. Estimates from laboratory and field measurements suggest that the contribution of damage and other  
off-fault processes to dissipation may be relatively small, <10 % (Chester et al., 2005; Rockwell et al., 2009; Aben et al., 2019),  
however, this remains an area of active research. Since the off-fault damage would be rupture-dependent as well, adding it to  
the consideration of the breakdown energy would likely further reinforce the conclusion of this study that breakdown energy  
is not an intrinsic **fault** property but rather is rupture-dependent.

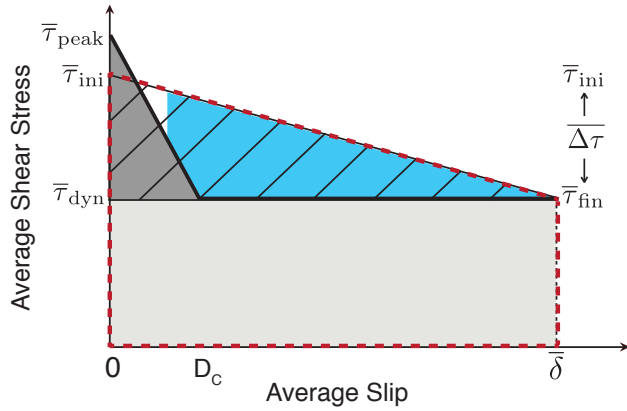
450

The finding that the breakdown energy - as well as the weakening rate - can vary substantially along a given rupture and  
among subsequent ruptures, even for comparable values of slip, suggests that caution is needed in using the inferred break-  
down energies from natural events for modeling of future earthquake scenarios. **Some dynamic rupture simulations account for  
thermo-hydro-mechanical effects (Andrews, 2002; Bizzarri and Cocco, 2006; Noda et al., 2009; Schmitt et al., 2015) and/or in-**  
455 **corporate the effects of inelastic off-fault damage (Dunham et al., 2011a, b; Roten et al., 2017; Withers et al., 2018) that should  
result in qualitatively similar effects on the breakdown energy. However, many employ simplified shear resistance evolutions  
that prescribe the breakdown energy and/or weakening rate directly, as a local fault property (Richards-Dinger and Dieterich,  
2012; Shaw et al., 2018; Gallovic et al., 2019; Dalguer et al., 2020). Future work is needed to investigate whether and how the  
complexity of the local weakening/strengthening behavior experienced by the simulated faults with thermo-hydro-mechanical  
460 and other mechanisms can be translated into simulations with more simplified local relations, e.g. slip-dependent, and still result  
in similar rupture dynamics.**

Furthermore, several features of faulting in the presence of thermo-hydro-mechanical effects call into question the overall  
analogy with cohesive-zone dynamic fracture theory and hence the significance of the breakdown energy as the quantity that  
465 controls rupture dynamics. The analogy between breakdown and fracture energies, and more broadly frictional faulting and  
shear cracks of traditional fracture mechanics, requires that the breakdown process be confined close to the rupture tip (small-  
scale yielding) and **that** the dynamic resistance level be constant; under such conditions, the conclusions of dynamic fracture  
theory apply, including on the significance of breakdown energy (Freund, 1990). However, neither of these assumptions holds  
for the faults with thermo-hydro-mechanical processes. The weakening - and hence breakdown process - typically continues  
470 with ongoing slip at seismic slip rates on such faults, long after the rupture front passes. As a result, the breakdown process is not  
confined to the rupture tip and the dynamic resistance level is not constant. Moreover, the total dissipated energy - not just the  
energy included in the notion of breakdown energy - contributes to shear heating and hence fault weakening in thermo-hydro-  
mechanical fault models. **That is why the entire dissipated energy may affect rupture dynamics as well.** These considerations  
emphasize the need for better understanding of rupture dynamics and its controls in the presence of thermo-hydro-mechanical  
475 processes and for more systematic incorporation of such processes in earthquake source modeling.

*Data availability.* The data supporting the analysis and conclusions are accessible through the CaltechDATA repository  
( <https://data.caltech.edu/records/1447> ).

(A) **Standard Slip-Weakening Energy Diagram**



(B)

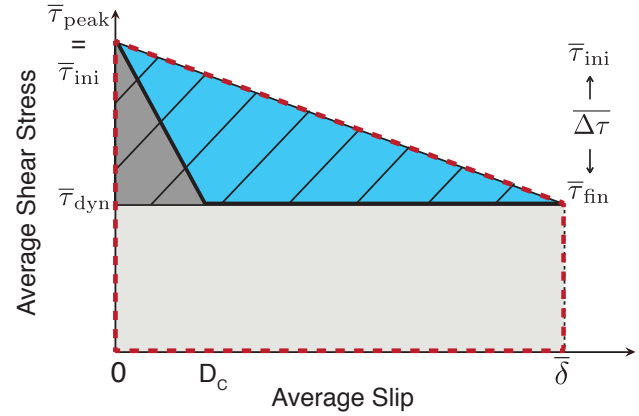


**Figure 1.** (A) Standard linear slip-weakening diagram where the **average** shear stress is assumed to increase from an initial to peak stress with no slip and then linearly decrease to a dynamic resistance level over a critical slip distance  $D_c$ . The difference between the average initial and final shear stress levels is called the static stress drop. The average stress vs. slip diagram is used to represent the energy partitioning of the total strain energy change per unit rupture area (dashed red trapezoid) into the breakdown energy (dark grey triangle), residual dissipated energy per unit area (light gray rectangle), and radiated energy per unit area (blue region). **The additional dissipation associated with the initial strengthening outside of the red trapezoid comes at expense of the radiated energy (white triangle inside the red-dashed trapezoid).** (B) **The case of the initial stress equal to the peak stress.** Note that this diagram is an approximation even if the local behavior is governed by linear slip-weakening friction, since different points of the rupture would have different slip, including near-zero slip close to the rupture edges, and averaging over the dynamic rupture would produce a different curve from the local behavior (Noda and Lapusta, 2012).

**Table 1.** Model parameters used in simulations of earthquakes and aseismic slip.

Parameter	Symbol	Value
Loading slip rate	$V_{pl}$	$10^{-9}$ m/s
Shear wave speed	$c_s$	3299 m/s
Shear modulus	$\mu$	36 GPa
Rate-and-state parameters		
Reference slip velocity	$V_*$	$10^{-6}$ m/s
Reference friction coefficient	$f_*$	0.6
Characteristic slip	$D_{RS}$	1 mm
Rate-and-state direct effect (VW)	$a$	0.010
Rate-and-state evolution effect (VW)	$b$	0.015
Rate-and-state direct effect (VS)	$a$	0.050
Rate-and-state evolution effect (VS)	$b$	0.003
Thermal pressurization parameters		
<b>Interseismic effective</b> normal stress	$\bar{\sigma} = (\sigma - p)$	25 MPa
Coupling coefficient (when TP present)	$\Lambda$	0.34 MPa/K
Thermal diffusivity	$\alpha_{th}$	$10^{-6}$ m <sup>2</sup> /s
Hydraulic diffusivity	$\alpha_{hy}$	$10^{-3}$ m <sup>2</sup> /s
Specific heat	$\rho c$	2.7 MPa/K
Shear zone half-width	$w$	10 mm
Length scales		
Fault length	$\lambda$	96 km
Frictional domain	$\lambda_{fr}$	72 km
Velocity-weakening region	$\lambda_{vw}$	24 km
Cell size	$\Delta z$	3.3 m
Quasi-static cohesive zone	$\Lambda_0$	75 m
Nucleation size (Rice & Ruina, 1983)	$h_{RR}^*$	200 m
Nucleation size (Rubin & Ampuero, 2005)	$h_{RA}^*$	490 m

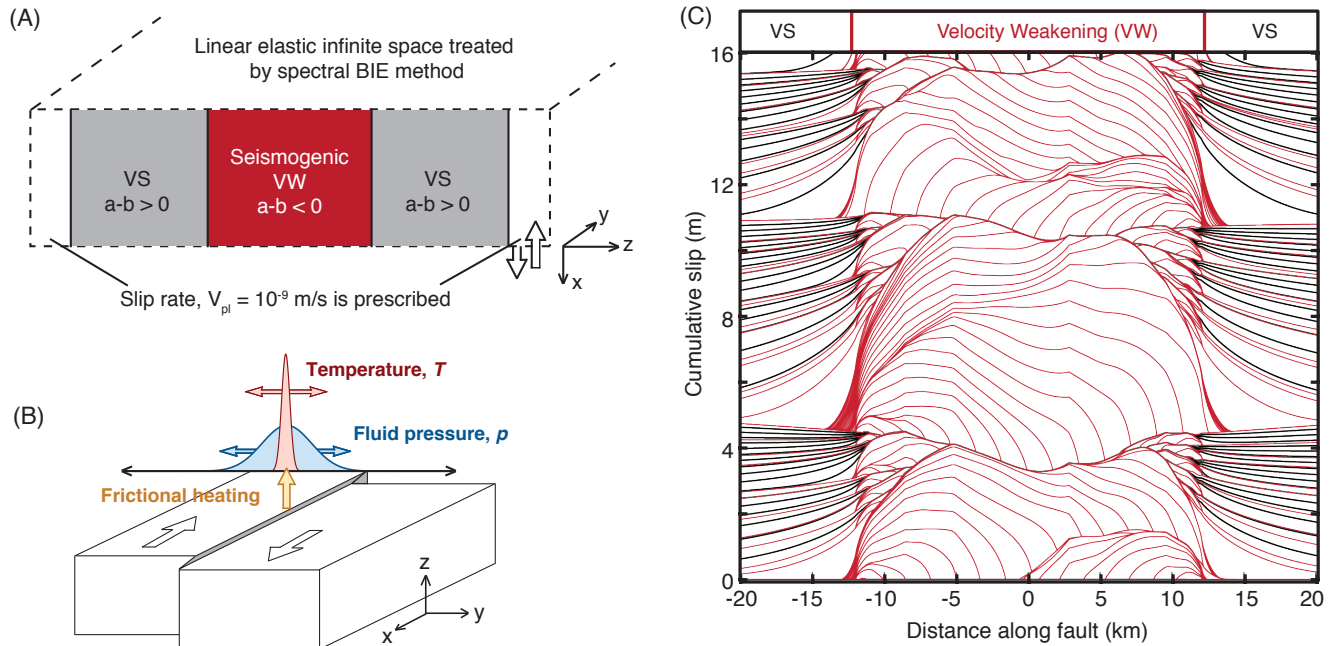


**Figure 2.** (A) The fault model incorporates a velocity-weakening (VW) seismogenic region surrounded by two velocity-strengthening (VS) sections. A fixed plate rate is prescribed outside of these regions. (B) We incorporate enhanced dynamic weakening due to the thermal pressurization of pore fluids by calculating the evolution of temperature and pore fluid pressure due to shear heating and off-fault diffusion throughout our simulations. (C) The beginning of the accumulated slip history for simulated sequences of crack-like earthquake ruptures and aseismic slip. Seismic events are illustrated by red lines with slip contours being plotted every 0.5 seconds while interseismic slip is plotted in black every 10 years. The total simulated slip history spans 2675 years corresponding to cumulative slip of 84 m and contains 200 seismic events.

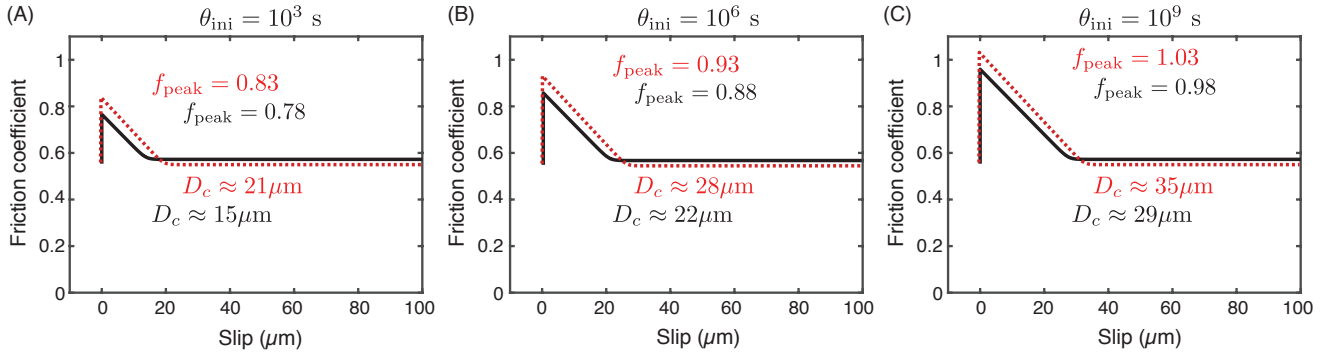


**Figure 3.** Illustration of the rate- and state-dependence of peak and dynamic friction coefficients,  $f_{\text{peak}}$  and  $f_{\text{dyn}}$  respectively, as well as the effective slip-weakening distance  $D_c$ . (A-C) Evolution of friction coefficient with slip for points with the same initial friction coefficient of 0.58 but different values of initial state variable  $\theta_{\text{ini}}$ , corresponding to different histories of previous motion. The initially locked point slips at an imposed slip rate of  $V = 1 \text{ cm/s}$  (black) or  $V = 1 \text{ m/s}$  (red), to approximately reproduce transition from the locked state to dynamic sliding as the rupture propagates through. For a given slip rate, the friction evolves to a new steady-state level,  $f_{\text{dyn}} = 0.54$  and  $f_{\text{dyn}} = 0.56$  for  $V = 1 \text{ m/s}$  and  $V = 1 \text{ cm/s}$ , respectively. These levels are similar, as expected from the logarithmic dependence on the slip rate and a narrow range of dynamic slip rates. The peak friction coefficient and effective slip-weakening distance vary more significantly with  $\theta_{\text{ini}}$ , where the peak friction coefficient increases for higher  $\theta_{\text{ini}}$  associated with longer inter-event healing times. The example uses typical laboratory values of  $(a - b) = 0.004$ ,  $f_* = 0.6$ ,  $L = 1 \mu\text{m}$ , and  $V_* = 10^{-6} \text{ m/s}$ .

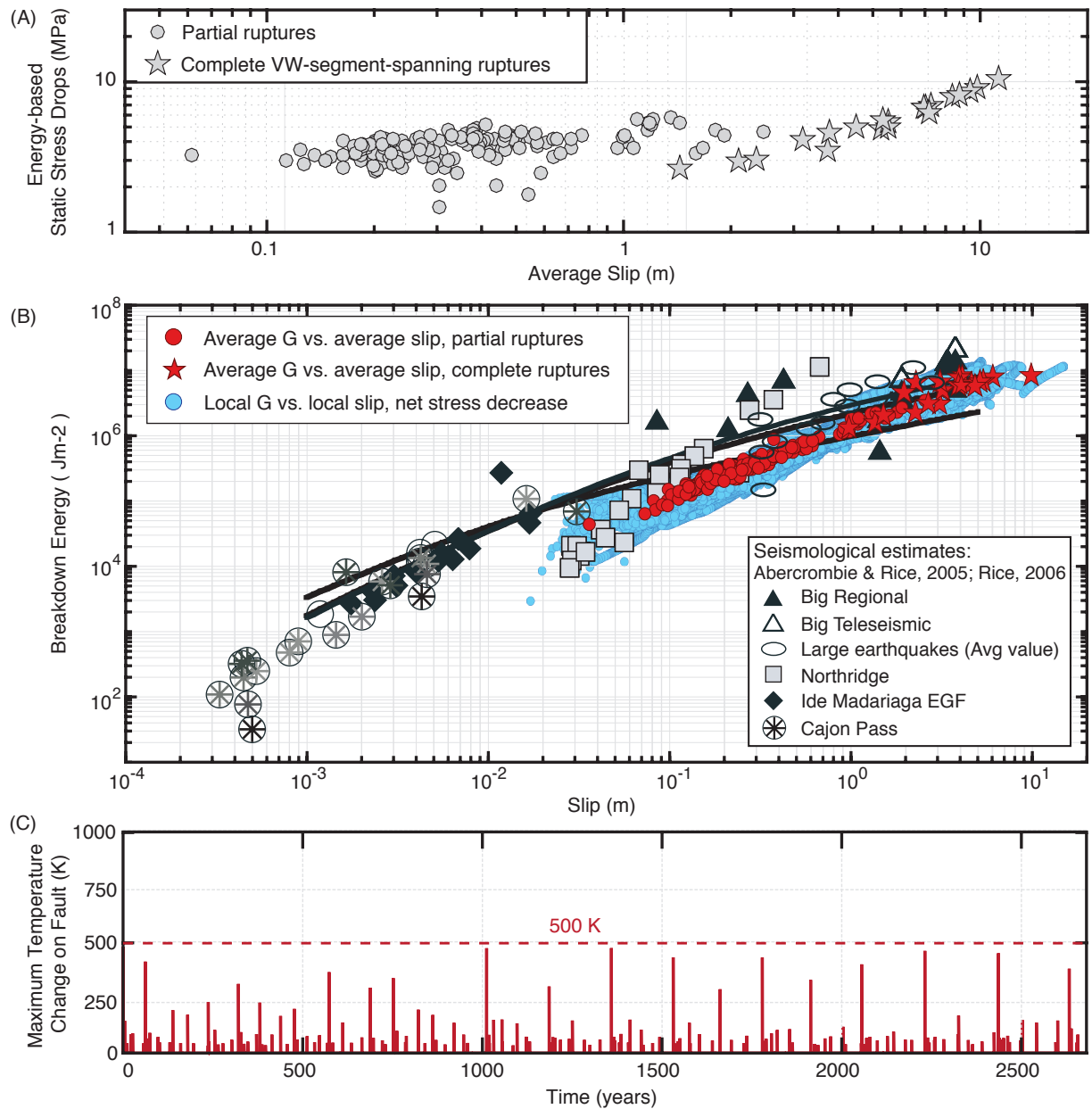


**Figure 4.** (A) The simulations result in a sequence of mostly crack-like ruptures that, despite including dynamic weakening due to thermal pressurization of pore fluids, are capable of reproducing nearly-magnitude invariant average static stress drops, with values between 1 - 10 MPa. (B) These crack-like ruptures display the overall increasing trend in average breakdown energy with average slip, as inferred for natural earthquakes (Abercrombie and Rice, 2005; Rice, 2006). (C) The simulated fault maintains reasonable temperatures and avoids melting, due to relatively low interseismic effective normal stress of 25 MPa (and hence chronic fluid overpressurization) and sufficiently efficient enhanced weakening due to thermal pressurization of pore fluids.

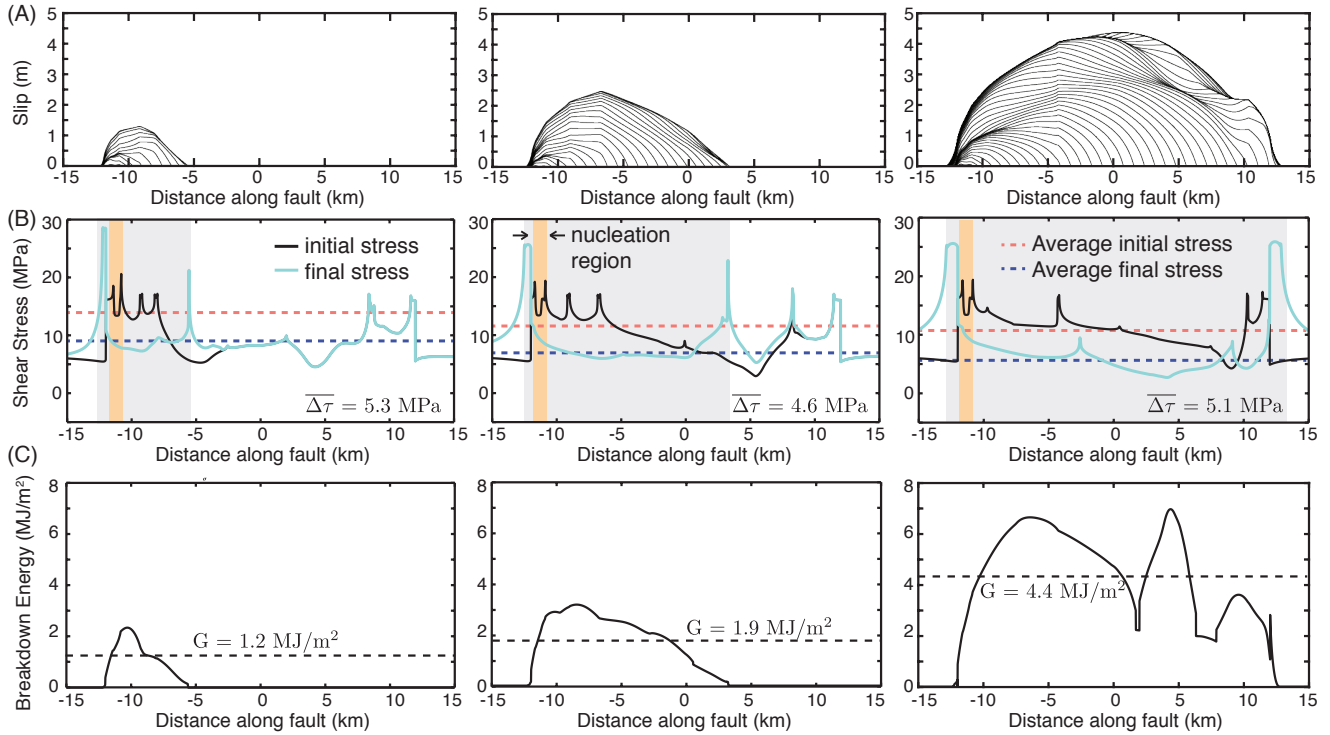


**Figure 5.** Comparison of three earthquake ruptures of different sizes nucleating over the same fault area. (A) Slip distributions for the three ruptures. (B) Distributions of initial (solid black) and final (solid blue) shear stress for the three ruptures. Gray shading denotes the ruptured region and orange shading denotes the region where each rupture nucleates. The dashed red and blue lines denote the average initial and final shear stress in the ruptured region. Large events have smaller initial and smaller final average stress, resulting in similar stress drops. (C) Distribution of breakdown energy (solid black) and average breakdown energy for each event (dashed line). The average breakdown energy generally increases with the rupture size.

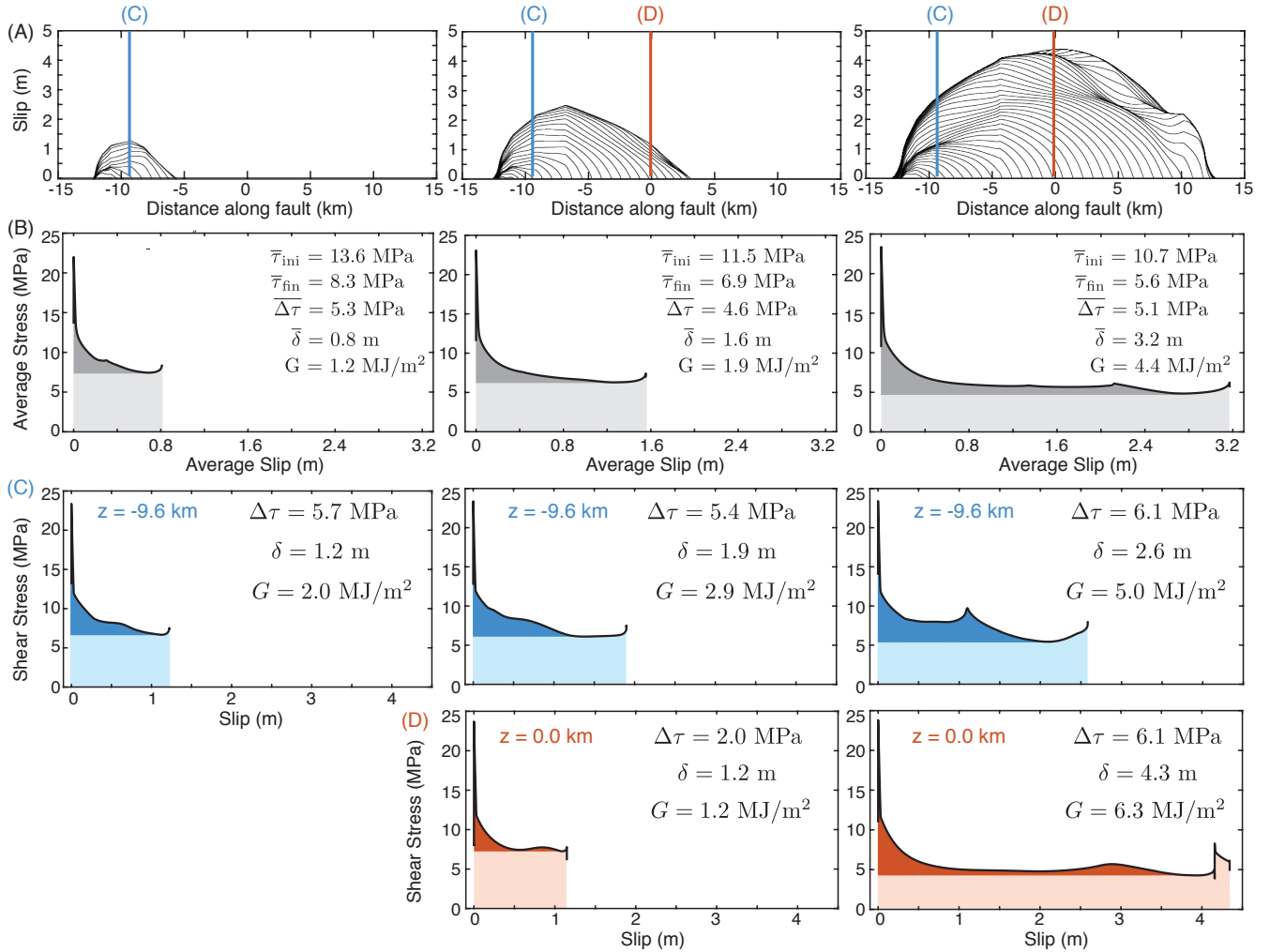


**Figure 6.** The dependence of shear stress on slip for the three ruptures of Figure 5. A) Slip distributions with locations examined in detail marked. (B) Average shear stress versus slip curves illustrating the energy partitioning of the ruptures, based on the averaging methodology of Noda and Lapusta (2012) that attempts to preserve local rupture behavior. The curves capture the continuous weakening with slip experienced by most rupture locations. (C-D) Local shear stress versus slip curves at two points within the three ruptures, illustrating the general trend in increasing breakdown energy with increasing slip at the same point.

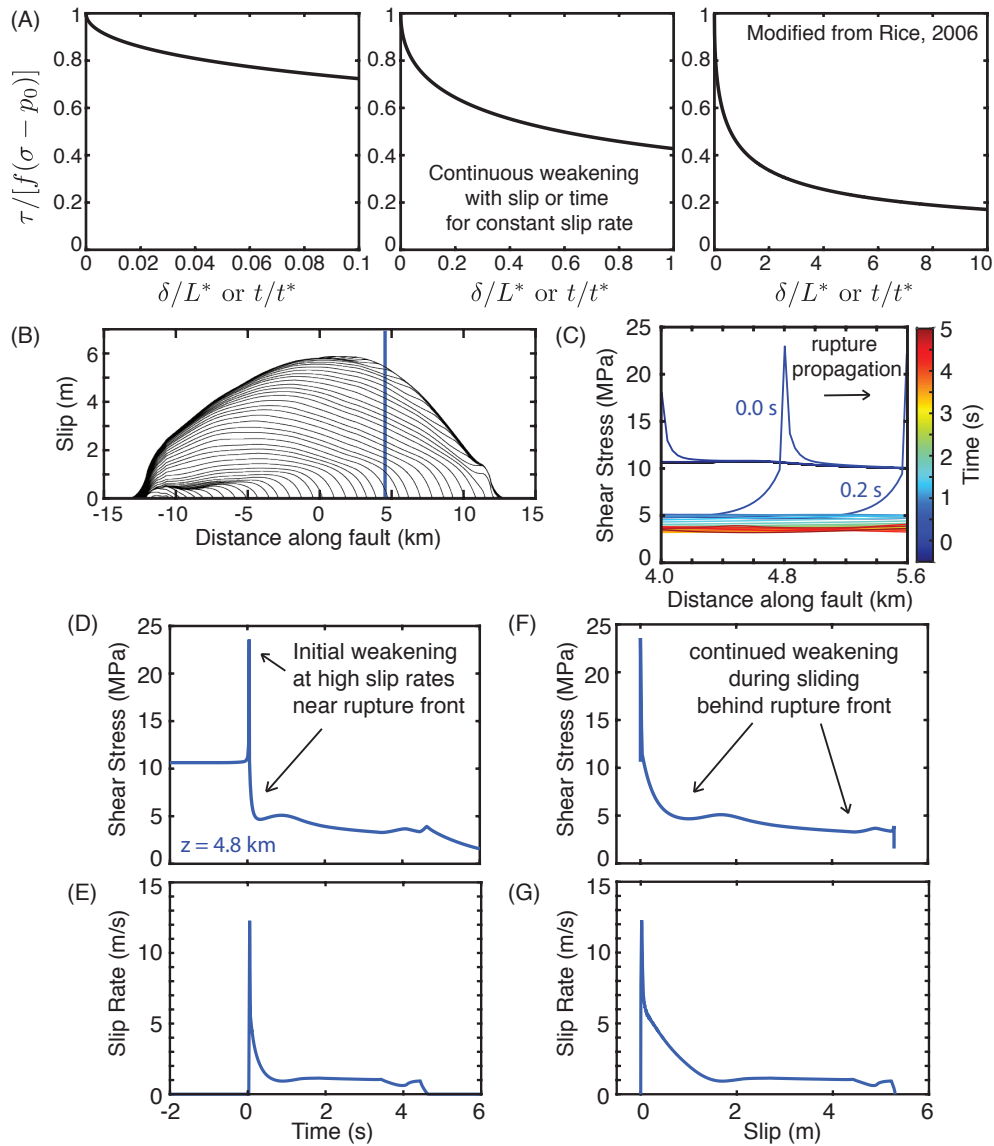


**Figure 7.** (A) Prediction of continuous weakening of shear resistance with slip or time due to the thermal pressurization of pore fluids during slip on a plane at constant slip rate  $V$  and constant friction coefficient  $f$  (Rice, 2006). (B) Evolution of slip during a dynamic rupture, slip contoured every 0.2 s. (C) Evolution of shear stress localized around the point  $z = 4.8$  km within the rupture. The time window shown corresponds to the duration of sliding at seismic slip rates at  $z = 4.8$  m. (D-E) Evolution of local shear stress and slip rate with time at the point indicated by the blue line in (B). (F-G) Evolution of local shear stress and slip rate with slip at the same point. While qualitatively consistent with (A) in terms of the continued weakening with slip and time, the evolution of shear resistance during dynamic ruptures depends on the more complicated history of slip rate, which varies throughout the rupture process. Most of the initial local weakening occurs at slip rates higher than 1 m/s as the rupture front passes by, followed by more gradual weakening behind the rupture front at lower, but still seismic, slip rates.

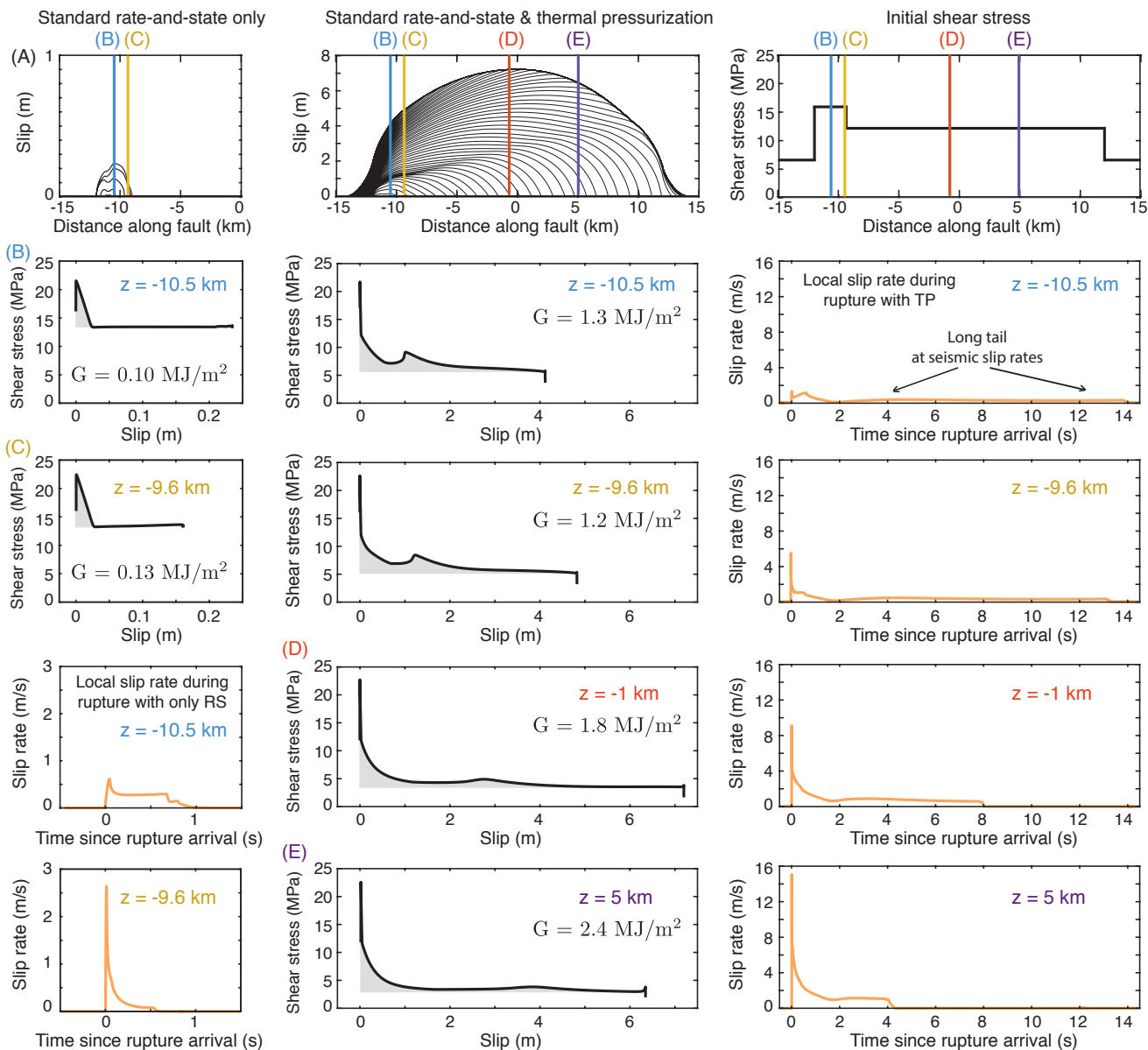


**Figure 8.** Comparison of accumulated slip, local shear stress vs. slip and local slip rate vs. time for ruptures with rate-and-state (RS) friction with and without enhanced weakening due to thermal pressurization (TP). The two ruptures occur with the same initial shear stress distribution (top right), which results in a relatively small rupture in the RS-only model that is localized within the relatively highly prestressed nucleation region (top left). The inclusion of TP allows the rupture to grow and propagate over lower prestress conditions (top center). (Left column) For the rupture governed by only RS, the breakdown of shear resistance is generally comparable at different locations with the same fault properties, despite differences in local slip rate. This is due to the relatively mild dependence of RS friction on slip rate. (Center and right columns) The rupture governed by RS and TP exhibits a more complex evolution of local shear stress and slip rate throughout the rupture, which depends not only on the local prestress but also the prestress and weakening behavior over the entire rupture through dynamic stress interactions.

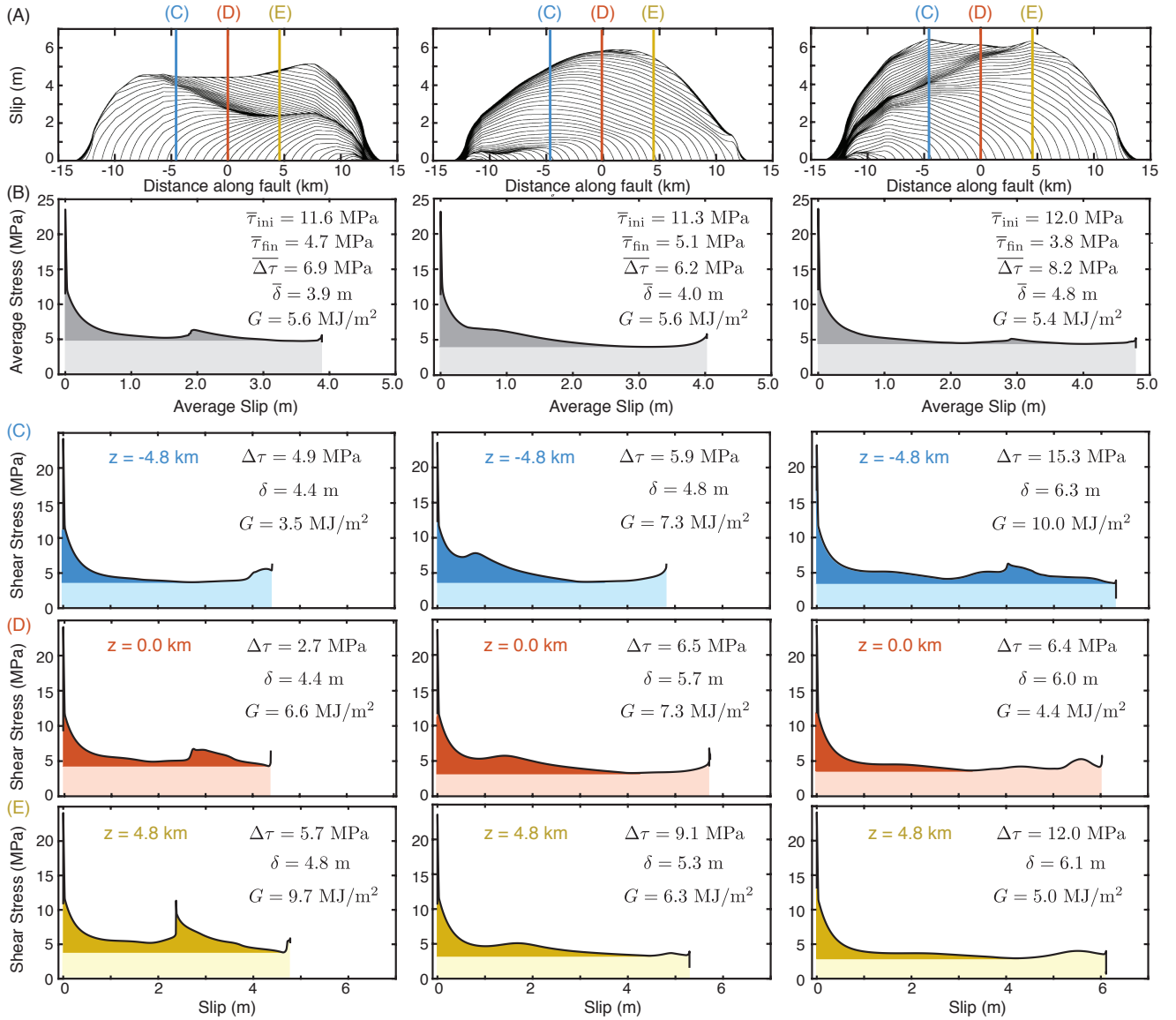


**Figure 9.** Comparison of local breakdown energy for three large earthquake ruptures with nearly the same average breakdown energy and comparable average slip. (A) Slip distributions for the three ruptures. (B) Average shear stress versus slip curves illustrating the energy partitioning of the ruptures. (C-E) Local shear stress versus slip curves at three points within the ruptures. There is not a strictly increasing trend of breakdown energy with slip for all points. In (C), the point  $z = -4.8$  km experiences increasing  $G$  with increasing slip. However, in (E), the point  $z = 4.8$  km experiences lower values of  $G$  in ruptures with larger local slip.

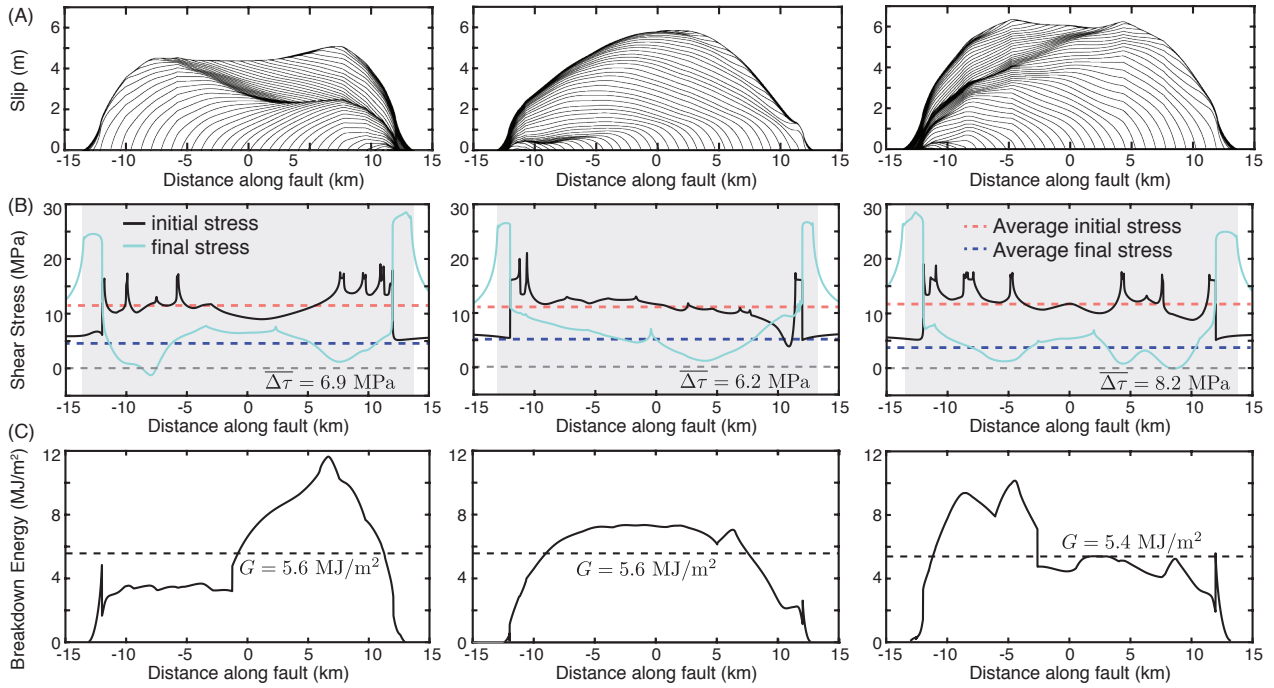


**Figure 10.** Comparison of the spatial breakdown energy distribution for the three large earthquake ruptures with nearly the same average breakdown energy and comparable average slip of Fig. 9. (A) Slip distributions for the three ruptures. (B) Spatial distributions of initial (solid black) and final (solid blue) shear stress for the three ruptures. Gray shading denotes the ruptured region and dashed red and blue lines indicate the average initial and final shear stresses, respectively. (C) Spatial distributions of the local breakdown energy. While the three ruptures have comparable average breakdown energy, the spatial variation throughout the rupture process considerably differs. Furthermore, the same spatial locations can have significantly different breakdown energy values in different rupture events of comparable size.

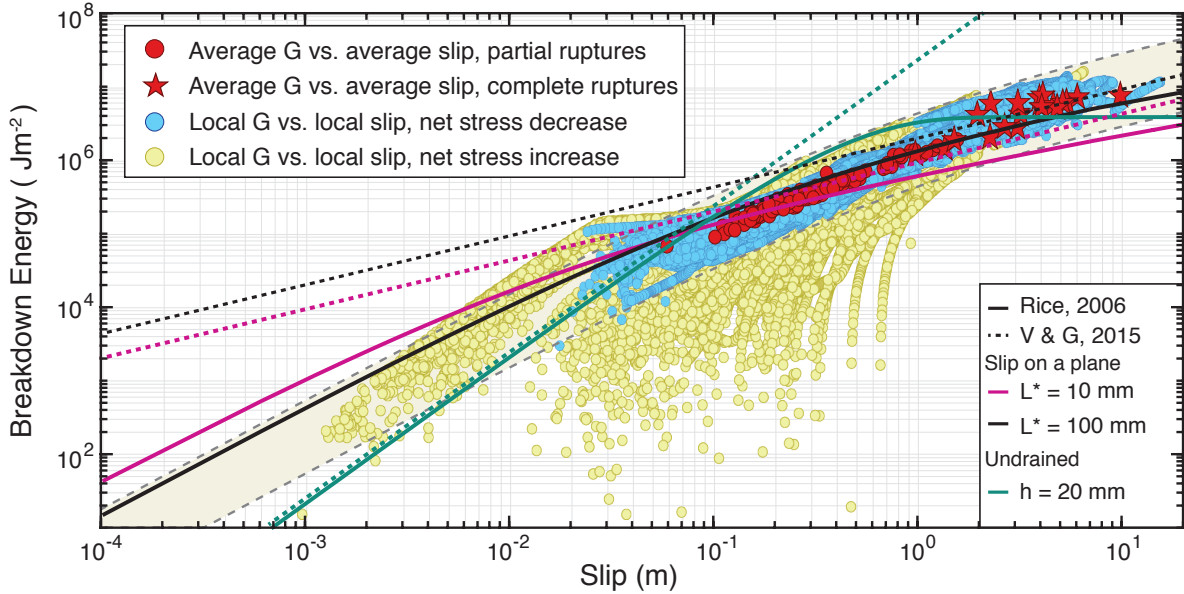


**Figure 11.** The average and local breakdown energy values for the simulated ruptures show an increasing trend with average and local slip, consistent with inferences from natural earthquakes (Fig. 4). The general trend of increasing breakdown energy with slip qualitatively holds for local points within our simulated ruptures; however, there is considerable variability for individual values of  $G$  at a given slip. For points that exhibit net weakening behavior in our simulated ruptures (blue circles), local values of  $G$  tend to vary within a factor of 3 from the scaling relationship between average  $G$  and average slip. The shaded band bordered by grey dashed lines illustrates the variation in  $G$  at a given value of slip. Local values of  $G$  are more variable for regions that experience a net increase in stress during the rupture process (yellow circles), e.g., regions close to rupture arrest. Theoretical curves for  $G$  vs. slip are indicated by solid lines for Eqs. (17) and (21) based on Rice (2006) and dashed lines for Eqs. (22 - 23) based on Viesca and Garagash (2015), with the coefficient of friction of  $f = 0.53$  and values otherwise indicated in Table 1. In both cases, the magenta and black lines correspond to the solutions for slip on a plane with two different values of  $L^*$  while the green line corresponds to the solution for an adiabatic and undrained shear band of width 20 mm.

*Author contributions.* V.L. and N.L. both contributed to developing the main ideas, designing the modeling, and producing the manuscript.  
480 V.L. carried out and analyzed the presented numerical experiments.

*Competing interests.* The authors declare no competing financial interests.

*Acknowledgements.* This study was supported by the National Science Foundation (grant EAR 1724686), the United States Geological Survey (grant G19AP00059), and the Southern California Earthquake Center (SCEC), contribution No. 19085. SCEC is funded by NSF Cooperative Agreement EAR-1033462 and USGS Cooperative Agreement G12AC20038. Numerical simulations for this study were carried  
485 out on the High Performance Computing Center cluster of the California Institute of Technology. **We thank Eric Dunham and Elisa Tinti for helpful comments and suggestions that improved the manuscript.**

## References

- Aben, F. M., Brantut, N., Mitchell, T. M., and David, E. C.: Rupture Energetics in Crustal Rock From Laboratory-Scale Seismic Tomography, *Geophysical Research Letters*, 46, 7337–7344, <https://doi.org/10.1029/2019GL083040>, 2019.
- 490 Abercrombie, R. E. and Rice, J. R.: Can observations of earthquake scaling constrain slip weakening?, *Geophysical Journal International*, 162, 406–424, <https://doi.org/10.1111/j.1365-246X.2005.02579.x>, 2005.
- Ampuero, J.-P. and Rubin, A. M.: Earthquake nucleation on rate and state faults – Aging and slip laws, *Journal of Geophysical Research: Solid Earth*, 113, <https://doi.org/10.1029/2007JB005082>, 2008.
- Andrews, D.: A fault constitutive relation accounting for thermal pressurization of pore fluid, *Journal of Geophysical Research: Solid Earth*, 495 107, 2002.
- Andrews, D. J.: Rupture dynamics with energy loss outside the slip zone, *Journal of Geophysical Research*, 110, <https://doi.org/10.1029/2004JB003191>, 2005.
- Aochi, H. and Ide, S.: Conceptual multi-scale dynamic rupture model for the 2011 off the Pacific coast of Tohoku Earthquake, *Earth, Planets and Space*, 63, 46, <https://doi.org/10.5047/eps.2011.05.008>, 2011.
- 500 Barbot, S., Lapusta, N., and Avouac, J.-P.: Under the hood of the earthquake machine: Toward predictive modeling of the seismic cycle, *Science*, 336, 707–710, 2012.
- Barras, F., Aldam, M., Roch, T., Brener, E. A., Bouchbinder, E., and Molinari, J.-F.: Emergence of Cracklike Behavior of Frictional Rupture: The Origin of Stress Drops, *Phys. Rev. X*, 9, 041 043, <https://doi.org/10.1103/PhysRevX.9.041043>, 2019.
- Bhattacharya, P., Rubin, A. M., Bayart, E., Savage, H. M., and Marone, C.: Critical evaluation of state evolution laws in rate and state friction: 505 Fitting large velocity steps in simulated fault gouge with time-, slip-, and stress-dependent constitutive laws, *Journal of Geophysical Research: Solid Earth*, 120, 6365–6385, <https://doi.org/10.1002/2015JB012437>, 2015.
- Bhattacharya, P., Rubin, A. M., and Beeler, N. M.: Does fault strengthening in laboratory rock friction experiments really depend primarily upon time and not slip?, *Journal of Geophysical Research: Solid Earth*, 122, 6389–6430, <https://doi.org/10.1002/2017JB013936>, 2017.
- Bizzarri, A. and Cocco, M.: A thermal pressurization model for the spontaneous dynamic rupture propagation on a three-dimensional fault: 510 1. Methodological approach, *Journal of Geophysical Research: Solid Earth*, 111, <https://doi.org/10.1029/2005JB003862>, 2006.
- Bouchon, M.: The state of stress on some faults of the San Andreas System as inferred from near-field strong motion data, *Journal of Geophysical Research: Solid Earth*, 102, 11 731–11 744, <https://doi.org/10.1029/97JB00623>, 1997.
- Bouchon, M., Sekiguchi, H., Irikura, K., and Iwata, T.: Some characteristics of the stress field of the 1995 Hyogo-ken Nanbu (Kobe) earthquake, *Journal of Geophysical Research: Solid Earth*, 103, 24 271–24 282, <https://doi.org/10.1029/98JB02136>, 1998.
- 515 Brantut, N. and Viesca, R. C.: The fracture energy of ruptures driven by flash heating, *Geophysical Research Letters*, 44, 6718–6725, <https://doi.org/10.1002/2017GL074110>, 2017.
- Brune, J. N., Henyey, T. L., and Roy, R. F.: Heat flow, stress, and rate of slip along the San Andreas fault, California, *Journal of Geophysical Research*, 74, 3821–3827, 1969.
- Causse, M., Dalguer, L. A., and Mai, P. M.: Variability of dynamic source parameters inferred from kinematic models of past earthquakes, 520 *Geophysical Journal International*, 196, 1754–1769, <https://doi.org/10.1093/gji/ggt478>, 2013.
- Chen, T. and Lapusta, N.: Scaling of small repeating earthquakes explained by interaction of seismic and aseismic slip in a rate and state fault model, *Journal of Geophysical Research*, 114, <https://doi.org/10.1029/2008JB005749>, 2009.

- Chester, J. S., Chester, F. M., and Kronenberg, A. K.: Fracture surface energy of the Punchbowl fault, San Andreas system, *Nature*, 437, 133, 2005.
- 525 Cocco, M. and Bizzarri, A.: On the slip-weakening behavior of rate- and state dependent constitutive laws, *Geophysical Research Letters*, 29, <https://doi.org/10.1029/2001GL013999>, 2002.
- Cocco, M. and Tinti, E.: Scale dependence in the dynamics of earthquake propagation: Evidence from seismological and geological observations, *Earth and Planetary Science Letters*, 273, 123 – 131, <https://doi.org/https://doi.org/10.1016/j.epsl.2008.06.025>, 2008.
- Cruz-Atienza, V. M., Olsen, K. B., and Dalguer, L. A.: Estimation of the Breakdown Slip from Strong-Motion Seismograms: Insights from  
530 Numerical Experiments, *Bulletin of the Seismological Society of America*, 99, 3454–3469, <https://doi.org/10.1785/0120080330>, 2009.
- Dalguer, L. A., Wu, H., Matsumoto, Y., Irikura, K., Takahama, T., and Tonagi, M.: Development of Dynamic Asperity Models to Predict Surface Fault Displacement Caused by Earthquakes, *Pure and Applied Geophysics*, 177, 1983–2006, <https://doi.org/10.1007/s00024-019-02255-8>, <https://doi.org/10.1007/s00024-019-02255-8>, 2020.
- Di Toro, G., Han, R., Hirose, T., De Paola, N., Nielsen, S., Mizoguchi, K., Ferri, F., Cocco, M., and Shimamoto, T.: Fault lubrication during  
535 earthquakes, *Nature*, 471, 494, 2011.
- Dieterich, J.: Applications of Rate- and State-Dependent Friction to Models of Fault Slip and Earthquake Occurrence, in: *Treatise on Geophysics*, edited by Schubert, G., pp. 107 – 129, Elsevier, Amsterdam, <https://doi.org/https://doi.org/10.1016/B978-044452748-6.00065-1>, 2007.
- Dieterich, J. H.: Modeling of Rock Friction 1. Experimental Results and Constitutive Equations, *Journal of Geophysical Research*, 84,  
540 2161–2168, 1979.
- Dunham, E. M., Belanger, D., Cong, L., and Kozdon, J. E.: Earthquake Ruptures with Strongly Rate-Weakening Friction and Off-Fault Plasticity, Part 1: Planar Faults, *Bulletin of the Seismological Society of America*, 101, 2296–2307, <https://doi.org/10.1785/0120100075>, 2011a.
- Dunham, E. M., Belanger, D., Cong, L., and Kozdon, J. E.: Earthquake Ruptures with Strongly Rate-Weakening Friction  
545 and Off-Fault Plasticity, Part 2: Nonplanar Faults, *The Bulletin of the Seismological Society of America*, 101, 2308–2322, <https://doi.org/10.1785/0120100076>, 2011b.
- Freund, L. B.: *Dynamic Fracture Mechanics*, Cambridge Monographs on Mechanics, Cambridge University Press, <https://doi.org/10.1017/CBO9780511546761>, 1990.
- Galovic, F., Valentova, L., Ampuero, J.-P., and Gabriel, A.-A.: Bayesian Dynamic Finite-Fault Inversion: 2. Application to the 2016 Mw  
550 6.2 Amatrice, Italy, Earthquake, *Journal of Geophysical Research: Solid Earth*, 124, 6970–6988, <https://doi.org/10.1029/2019JB017512>, 2019.
- Goldsby, D. L. and Tullis, T. E.: Flash Heating Leads to Low Frictional Strength of Crustal Rocks at Earthquake Slip Rates, *Science*, 334, 216–218, <https://doi.org/10.1126/science.1207902>, 2011.
- Guatteri, M. and Spudich, P.: What Can Strong-Motion Data Tell Us about Slip-Weakening Fault-Friction Laws?, *Bulletin of the Seismological Society of America*, 90, 98–116, <https://doi.org/10.1785/0119990053>, 2000.
- Heaton, T. H.: Evidence for and implications of self-healing pulses of slip in earthquake rupture, *Physics of the Earth and Planetary Interiors*, 64, 1–20, 1990.
- Hickman, S. and Zoback, M.: Stress orientations and magnitudes in the SAFOD pilot hole, *Geophysical Research Letters*, 31, 2004.
- Ida, Y.: Cohesive force across the tip of a longitudinal-shear crack and Griffith's specific surface energy, *Journal of Geophysical Research*,  
560 77, 3796–3805, 1972.

- Ide, S. and Aochi, H.: Earthquakes as multiscale dynamic ruptures with heterogeneous fracture surface energy, *Journal of Geophysical Research: Solid Earth*, 110, <https://doi.org/10.1029/2004JB003591>, 2005.
- Ide, S. and Takeo, M.: Determination of constitutive relations of fault slip based on seismic wave analysis, *Journal of Geophysical Research: Solid Earth*, 102, 27 379–27 391, <https://doi.org/10.1029/97JB02675>, 1997.
- 565 Jiang, J. and Lapusta, N.: Deeper penetration of large earthquakes on seismically quiescent faults, *Science*, 352, 1293–1297, <https://doi.org/10.1126/science.aaf1496>, 2016.
- Kanamori, H. and Brodsky, E. E.: The Physics of Earthquakes, *Reports on Progress in Physics*, 67, 1429–1496, <https://doi.org/10.1088/0034-4885/67/8/R03>, 2004.
- Kanamori, H. and Heaton, T. H.: Microscopic and macroscopic physics of earthquakes, *Geocomplexity and the Physics of Earthquakes*, pp. 147–163, 2000.
- 570 Kanamori, H. and Rivera, L.: Energy Partitioning during an earthquake, *Earthquakes: Radiated energy and the physics of faulting*, pp. 3–13, 2006.
- Kaneko, Y., Fukuyama, E., and Hamling, I. J.: Slip-weakening distance and energy budget inferred from near-fault ground deformation during the 2016 Mw 7.8 Kaikura earthquake, *Geophysical Research Letters*, 44, 4765–4773, <https://doi.org/10.1002/2017GL073681>, 2017.
- 575 Kostrov, B. V. and Das, S.: Principles of earthquake source mechanics, Cambridge, England ; New York : Cambridge University Press, 1988.
- Lachenbruch, A. H. and Sass, J. H.: Heat flow and energetics of the San Andreas Fault Zone, *Journal of Geophysical Research: Solid Earth*, 85, 6185–6222, <https://doi.org/10.1029/JB085iB11p06185>, 1980.
- Lambert, V., Lapusta, N., and Perry, S.: Do large earthquakes propagate as self-healing pulses or mild cracks?, *Nature*, in review.
- Lapusta, N. and Liu, Y.: Three-dimensional boundary integral modeling of spontaneous earthquake sequences and aseismic slip, *Journal of Geophysical Research*, 114, B09 303, <https://doi.org/10.1029/2008JB005934>, 2009.
- 580 Lapusta, N., Rice, J. R., Ben-Zion, Y., and Zheng, G.: Elastodynamic Analysis for Slow Tectonic Loading with Spontaneous Rupture Episodes on Faults with Rate- and State- dependent Friction, *Journal of Geophysical Research*, 105, 765–789, <https://doi.org/10.1029/2000JB900250>, 2000.
- Madariaga, R.: Dynamics of an Expanding Circular Fault, *Bulletin of the Seismological Society of America*, 66, 639–666, 1976.
- 585 Mase, C. W. and Smith, L.: The role of pore fluids in tectonic processes, *Reviews of Geophysics*, 25, 1348–1358, <https://doi.org/10.1029/RG025i006p01348>, 1987.
- Nielsen, S., Spagnuolo, E., Violay, M., Smith, S., Di Toro, G., and Bistacchi, A.: G: Fracture energy, friction and dissipation in earthquakes, *Journal of Seismology*, 20, 1187–1205, <https://doi.org/10.1007/s10950-016-9560-1>, 2016.
- Noda, H. and Lapusta, N.: Three-dimensional earthquake sequence simulations with evolving temperature and pore pressure due to shear heating: Effect of heterogeneous hydraulic diffusivity, *Journal of Geophysical Research*, 115, B123 414, <https://doi.org/10.1029/2010JB007780>, 2010.
- 590 Noda, H. and Lapusta, N.: On Averaging Interface Response During Dynamic Rupture and Energy Partitioning Diagrams for Earthquakes, *Journal of Applied Mechanics*, 79, <https://doi.org/10.1115/1.4005964>, 2012.
- Noda, H. and Lapusta, N.: Stable creeping fault segments can become destructive as a result of dynamic weakening, *Nature*, 493, 518 EP –, 2013.
- 595 Noda, H., Dunham, E. M., and Rice, J. R.: Earthquake ruptures with thermal weakening and the operation of major faults at low overall stress levels, *Journal of Geophysical Research: Solid Earth*, 114, <https://doi.org/10.1029/2008JB006143>, 2009.

- Noda, H., Lapusta, N., and Kanamori, H.: Comparison of average stress drop measures for ruptures with heterogeneous stress change and implications for earthquake physics, *Geophysical Journal International*, <https://doi.org/10.1093/gji/ggt074>, 2013.
- 600 Okubo, K., Bhat, H. S., Rougier, E., Marty, S., Schubnel, A., Lei, Z., Knight, E. E., and Klinger, Y.: Dynamics, Radiation, and Overall Energy Budget of Earthquake Rupture With Coseismic Off-Fault Damage, *Journal of Geophysical Research: Solid Earth*, 124, 11 771–11 801, <https://doi.org/10.1029/2019JB017304>, 2019.
- Okubo, P. G.: Dynamic rupture modeling with laboratory-derived constitutive relations, *Journal of Geophysical Research: Solid Earth*, 94, 12 321–12 335, <https://doi.org/10.1029/JB094iB09p12321>, 1989.
- 605 Olsen, K. B., Madariaga, R., and Archuleta, R. J.: Three-Dimensional Dynamic Simulation of the 1992 Landers Earthquake, *Science*, 278, 834–838, <https://doi.org/10.1126/science.278.5339.834>, 1997.
- Palmer, A. C. and Rice, J.: The growth of slip surfaces in the progressive failure of over-consolidated clay, *Proceedings of the Royal Society of London A: Mathematical, Physical and Engineering Sciences*, 332, 527–548, 1973.
- Passelegue, F. X., Goldsby, D. L., and Fabbri, O.: The influence of ambient fault temperature on flash-heating phenomena, *Geophysical*  
610 *Research Letters*, 41, 828–835, <https://doi.org/10.1002/2013GL058374>, 2014.
- Perry, S. M., Lambert, V., and Lapusta, N.: Nearly magnitude-invariant stress drops in simulated crack-like earthquake sequences on rate-and-state faults with thermal pressurization of pore fluids, *Journal of Geophysical Research: Solid Earth*, 125, e2019JB018 597, <https://doi.org/10.1029/2019JB018597>, 2020.
- Poliakov, A. N. B., Dmowska, R., and Rice, J. R.: Dynamic shear rupture interactions with fault bends and off-axis secondary faulting,  
615 *Journal of Geophysical Research: Solid Earth*, 107, ESE 6–1–ESE 6–18, <https://doi.org/10.1029/2001JB000572>, 2002.
- Rice, J.: Flash heating at asperity contacts and rate-dependent friction, *Eos Trans. AGU*, 80, F471, 1999.
- Rice, J.: Fracture energy of earthquakes and slip-weakening rupture parameters, *EOS, Trans. Am. geophys. Un., Fall Meeting Suppl*, 81, F1227, 2000.
- Rice, J. and Ruina, A. L.: Stability of steady frictional slipping, *Journal of Applied Mechanics*, 50, 343–349, 1983.
- 620 Rice, J. R.: The Mechanics of Earthquake Rupture, in *Physics of Earth's Interior*, pp. 555–649, 1980.
- Rice, J. R.: Heating and weakening of faults during earthquake slip, *Journal of Geophysical Research*, 111, B05 311, <https://doi.org/10.1029/2005JB004006>, 2006.
- Rice, J. R., Lapusta, N., and Ranjith, K.: Rate and state dependent friction and the stability of sliding between elastically deformable solids, *Journal of the Mechanics and Physics of Solids*, 49, 1865–1898, 2001.
- 625 Richards-Dinger, K. and Dieterich, J. H.: RSQSim Earthquake Simulator, *Seismological Research Letters*, 83, 983–990, <https://doi.org/10.1785/0220120105>, 2012.
- Rockwell, T., Sisk, M., Girty, G., Dor, O., Wechsler, N., and Ben-Zion, Y.: Chemical and Physical Characteristics of Pulverized Tejon Lookout Granite Adjacent to the San Andreas and Garlock Faults: Implications for Earthquake Physics, *Pure and Applied Geophysics*, 166, 1725–1746, <https://doi.org/10.1007/s00024-009-0514-1>, 2009.
- 630 Roten, D., Olsen, K. B., and Day, S. M.: Off-fault deformations and shallow slip deficit from dynamic rupture simulations with fault zone plasticity, *Geophysical Research Letters*, 44, 7733–7742, <https://doi.org/10.1002/2017GL074323>, 2017.
- Rubin, A. and Ampuero, J.-P.: Earthquake nucleation on (aging) rate and state faults, *Journal of Geophysical Research: Solid Earth*, 110, 2005.
- Ruina, A.: Slip Instability and State Variable Friction Laws, *Journal of Geophysical Research*, 88, 10 359–10 370, 1983.

- 635 Schmitt, S. V., Segall, P., and Dunham, E. M.: Nucleation and dynamic rupture on weakly stressed faults sustained by thermal pressurization, *Journal of Geophysical Research: Solid Earth*, 120, 7606–7640, <https://doi.org/10.1002/2015JB012322>, 2015.
- Selvadurai, P. A.: Laboratory Insight Into Seismic Estimates of Energy Partitioning During Dynamic Rupture: An Observable Scaling Breakdown, *Journal of Geophysical Research: Solid Earth*, 124, 11 350–11 379, <https://doi.org/10.1029/2018JB017194>, 2019.
- Shaw, B. E., Milner, K. R., Field, E. H., Richards-Dinger, K., Gilchrist, J. J., Dieterich, J. H., and Jordan, T. H.: A physics-based earthquake simulator replicates seismic hazard statistics across California, *Science Advances*, 4, <https://doi.org/10.1126/sciadv.aau0688>, 2018.
- 640 Shreedharan, S., Riviere, J., Bhattacharya, P., and Marone, C.: Frictional State Evolution During Normal Stress Perturbations Probed With Ultrasonic Waves, *Journal of Geophysical Research: Solid Earth*, 124, 5469–5491, <https://doi.org/10.1029/2018JB016885>, 2019.
- Sibson, R. H.: Interactions between temperature and pore-fluid pressure during earthquake faulting and a mechanism for partial or total stress relief., *Nature*, 243, 66–68, 1973.
- 645 Sibson, R. H.: Generation of Pseudotachylyte by Ancient Seismic Faulting, *Geophysical Journal of the Royal Astronomical Society*, 43, 775–794, <https://doi.org/10.1111/j.1365-246X.1975.tb06195.x>, 1975.
- Tinti, E., Spudich, P., and Cocco, M.: Earthquake fracture energy inferred from kinematic rupture models on extended faults, *Journal of Geophysical Research: Solid Earth*, 110, <https://doi.org/10.1029/2005JB003644>, 2005.
- Tullis, T.: Friction of Rock at Earthquake Slip Rates, *Treatise on Geophysics*, 4, 131–152, <https://doi.org/10.1016/B978-044452748-6.00064-X>, 2007.
- 650 Viesca, R. C. and Garagash, D. I.: Ubiquitous weakening of faults due to thermal pressurization, *Nature Geoscience*, 8, 875–879, <https://doi.org/10.1038/NGEO2554>, 2015.
- Williams, C. F., Grubb, F. V., and Galanis, S. P.: Heat flow in the SAFOD pilot hole and implications for the strength of the San Andreas Fault, *Geophysical Research Letters*, 31, 2004.
- 655 Withers, K. B., Olsen, K. B., Day, S. M., and Shi, Z.: Ground Motion and Intraevent Variability from 3D Deterministic Broad-band (0-7.5 Hz) Simulations along a Nonplanar Strike-Slip Fault, *Bulletin of the Seismological Society of America*, 109, 229–250, <https://doi.org/10.1785/0120180006>, <https://doi.org/10.1785/0120180006>, 2018.
- Zoback, M. D., Zoback, M. L., Mount, V. S., Suppe, J., Eaton, J. P., Healy, J. H., Oppenheimer, D., Reasenber, P., Jones, L., Raleigh, C. B., Wong, I. G., Scotti, O., and Wentworth, C.: New Evidence on the State of Stress of the San Andreas Fault System, *Science*, 238, 1105–1111, <https://doi.org/10.1126/science.238.4830.1105>, 1987.
- 660